



Research article

The technical challenges and outcomes of ground-penetrating radar: A site-specific example from Joggins, Nova Scotia

Trevor B. Kelly^{1,*}, Grant D. Wach¹ and Darragh E. O'Connor^{1,2}

¹ Department of Earth and Environmental Sciences, Dalhousie University, Halifax, NS, Canada

² Department of Earth and Environmental Sciences, University of Manchester, Manchester, ENG, United Kingdom

* **Correspondence:** Email: tbkelly@dal.ca.

Abstract: The Carboniferous Joggins Formation is known for its complete succession of fossil-rich, coal-bearing strata, deposited in a fluvial meanderbelt depositional setting. Hence, the Joggins Formation outcrop is an excellent analogue for studying the 2D geological complexities associated with meanderbelt systems. In this research, a conventional ground-penetrating radar system was tested with the intent of imaging near-surface, dipping, strata of the Joggins Formation (potentially with subsequent repeats as annual erosion provides new visual calibrations). The survey was unsuccessful in its primary goal, and for future reference we document the reasons here. However, the overlying near-surface angular unconformity was successfully imaged enabling mapping of the approximately 8 m of overlying glacial till. A successful outcome would have allowed observations from the 2D outcrop to be extended into 3D space and perhaps lead to an increased understanding of the small (e.g., bedform baffles and barriers) and large (e.g., channel bodies) scale architectural elements, meanderbelt geometry, and aspect ratios. The study comprises a 42-line, 3.46 km ground-penetrating radar survey using a Sensors and Software pulseEKKO Pro SmartCart system. It was combined with a real-time kinematic differential global positioning system for the georeferencing of survey lines. The 50 MHz antenna frequency, with a 1 m separation, was chosen to maximize the depth of penetration, while still maintaining a reasonable resolution. The results show that many of the lines are contaminated with diffraction hyperbolae, possibly caused from buried objects near or under the survey lines or surface objects near the survey lines. A total of thirteen unique radar reflectors are described and interpreted from this work. The thick clay-rich soil overlying the Joggins Formation probably contributed to

significant signal attenuation and the nature of the Carboniferous strata (dip of the beds, pinching and swelling of the beds, bed thickness, etc.) also contributed to imaging difficulties.

Keywords: 2D; attenuation; near-surface geophysics; non-destructive; heterogeneity

1. Introduction

The use of 2D siliclastic outcrops for the study of reservoir analogues provides a wealth of knowledge relating to the interwell scale geometrical and petrophysical heterogeneities within a depositional system, which ultimately control permeability and porosity, and thus, the mobility and capacity of reservoir fluids [1]. Ideally, the 2D outcrop would be extended into the third dimension to allow for the development of a continuous model that would further help with interpretations. The issue that one is then faced with is how to best fill in the region behind the outcrop to create a 3D model [2]. One such method that has the potential of providing this data is ground-penetrating radar (GPR); a near-surface geophysical technique that can provide high-resolution images of ancient and modern sedimentary sequences, which can be used to improve the understanding of small (e.g., bedform baffles and barriers) to large (e.g., channel bodies) scale architectural elements, meanderbelt geometry, and aspect ratios, just to name a few [1–11].

GPR is a non-invasive and non-destructive remote sensing geophysical technique that is highly useful and versatile utilized in several different disciplines for the imaging and subsequent study of the shallow subsurface (e.g., [12,13]). It accomplishes this through the detection of electrical discontinuities by the generation, propagation, reflection, and reception of pulsed high-frequency electromagnetic energy (e.g., [12,13]). These discontinuities are directly related to water saturation, salinity, porosity, and mineralogical variations [3,14]. Ideal GPR results are typically achieved from clean, quartzose-rich clastic sediments that contain no clays or silts (e.g., [7,15]). Signal attenuation is a real concern when performing a GPR survey, with problems arising from concentrations of silt, clay, caliche, and moist saline conditions (e.g., [7,15,16]).

Here we provide the first comprehensive results from a primarily road-based GPR survey. In this study, a total of 42 GPR lines were collected over the Carboniferous-aged Joggins Formation of northern Nova Scotia, Canada, using one set of 50 MHz antennae arranged as a transmitter/receiver pair. The GPR system was combined with a Real-Time Kinematic (RTK) Differential Global Positioning System (DGPS) to provide a fully georeferenced group of survey lines with positional accuracy of approximately ± 2 cm [17]. The goals of this survey were to image the dipping conformable strata of the fluvial-dominated Joggins Formation to identify sedimentary structures that could be correlated with a previously obtained lidar survey of the cliff face. This work was performed with the aim of providing constraining data on the reservoir architecture of the Carboniferous fluvial meanderbelt system of the Joggins Formation in 3D (outcrop + GPR). The results of the GPR study were to be used as inputs to stochastic models of the Joggins Formation with the purpose of understanding the inherent reservoir heterogeneity sensitivities of the analogous reservoir. The four main geometric measures include channel depth, channel width, sandstone thickness and channel-belt

width. From those, four aspect ratios can be calculated, (1) channel depth versus sandstone thickness, (2) channel depth versus channel width, (3) channel-belt width versus channel depth, and (4) channel-belt width versus channel width. Gibling [18] documents the width and thickness of fluvial channel bodies from the geological record, including those measured from the 2D outcrop exposure of the Joggins Formation. Additionally, this study was carried out to test the applicability of the GPR system to provide high-resolution imaging of the dipping strata of the Joggins Formation, with the possibility that these images could be integrated with other outcrop (e.g., LiDAR) and subsurface data (e.g., drill core, well logs). The majority of the GPR data show strong diffraction hyperbolae, which is likely the result of above ground and subsurface objects. These objects could not be bypassed since most of the GPR lines were conducted on gravel/dirt roads traversing on top of the Joggins Formation strata. The objects that contaminate the radargrams must be understood and differentiated from the true sedimentary structures that were the purpose of this survey. There are also many other items that were unique to this survey that could potentially result in the radargrams being contaminated.

A search of previous research related to the Joggins Formation yields a vast number of publications that are either written directly about the Joggins Formation or mention the Joggins Formation in some capacity (e.g., [18–23]). According to a recent publication by Grey and Finkel [24], the bulk of the research occupies one of three major categories; a general geology category that includes sedimentology and stratigraphy publications (e.g., [21,22,25,26]); a paleobiology category that includes taxonomic discoveries and descriptions (e.g., [27–31]); and a paleoecology category (e.g., [20,32]). Despite the abundant research carried out in this area, there is a lack of research into the subsurface imaging of the Joggins Formation, particularly those that utilize ground penetrating radar. The exception dating back to the early 1960's, until approximately 2008, when numerous 2D seismic lines were collected in the onshore Cumberland Subbasin for the purpose of hydrocarbon resources exploration. In addition, several petroleum boreholes were drilled to test areas and structures of potential interest. Some of these wells penetrated the Joggins Formation strata. The Athol Syncline was the focus of a regional seismic study and appeared to show evidence of rapid subsidence within the Cumberland Subbasin resulting from Mississippian salt withdrawal at depth, allowing for thick sediment accumulations and preservation [26].

2. Study area

The community of Joggins is located approximately 230 km north of Halifax, Nova Scotia. Joggins and the corresponding outcrop lie alongside Chignecto Bay, a smaller bay within the grander Bay of Fundy. In this area, the tides ebb and flow some 13 m with each tidal cycle (Figure 1). The mean annual temperature is approximately 6.0 °C, and the mean annual precipitation is 1154.8 mm. The ease of access, continuity and quality of the Joggins Formation exposure and the numerous road/grass surfaces over which a GPR survey could be completed are the main reasons behind its selection as a study site. The Joggins Fossil Cliffs (Joggins Formation) were nominated in 2008 as a United Nations Educational, Scientific and Cultural Organization (UNESCO) heritage site, together with six additional conformable formations (Ragged Reef, Springhill Mines, Little River, Boss Point, Claremont and Shepody) because of the exceptionally well-preserved rock outcrops and fossil

assemblages that document life during the “Coal Age”, a time when fertile forests and wetlands occupied the World’s tropics [33].

Joggins and the nearby area have seen extensive coal mining that dates back to 1686 [34], continuing intermittently for over 200 years. During that time, elaborate underground mine workings were created, with many of the remnants (e.g., mine opening supports and railway line support timbers) visible in the cliff face from the intertidal zone (e.g., [34–36]). The surface development was also substantial, with timbers (rail track and support) and steel spikes still visible on the intertidal zone between Main Street and the Joggins Fossil Cliffs center. The remains of a wooden pier that existed for the load-out of coal onto ships during high tide for destinations throughout the Maritimes and New England [34]. The ground over which the GPR survey was conducted, has seen extensive, human-related activity, which needs to be accounted for when interpreting the data.

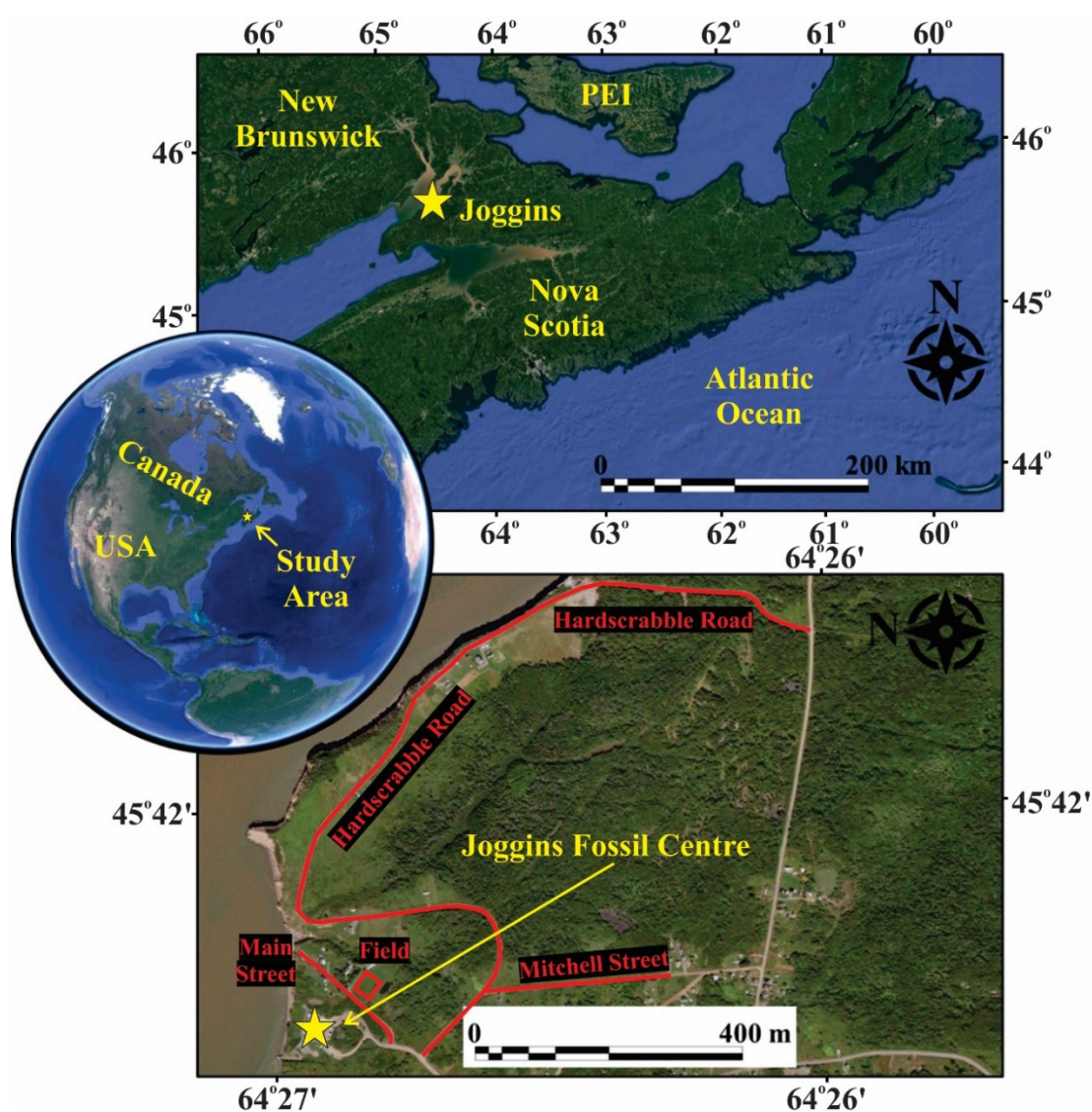


Figure 1. Location map of Joggins, Nova Scotia. GPR data was collected from the areas outlined with red (basemap from [37]).

3. Geological background

3.1. Overburden geology

Overburden (soil and glacial till) geology is important for GPR studies because of the direct impact it has on data collection, especially when attempting to image underlying bedrock. A review of borehole reports from the area describes the overburden as ranging in thickness from 1.5 to 20.1 m (average of 6.4 m). In the study area, the Joggins Formation is overlain by glacial till with a developed soil horizon on top for a total thickness of approximately 8 m (Figure 2). Joggins soils are grayish-brown, moderately fine-textured, and stony with poor internal drainage (e.g., [38,39]). The “A” horizon is at least 15 cm thick and characterized by pale gray to pale brown sandy loam and sandy clay loam with yellowish mottling, an indication of extended saturation and gleying (e.g., [38,39]). Underlying is a 10 to 25 cm thick yellowish and reddish interval of mottled material with a dullish brown matrix, manganese dioxide (MnO_2) concretions and considerable free iron accumulation. The remaining “B” horizon begins at approximately 30 cm and continues to 60 cm depth. It is a compact, dense sandy clay loam with a weakening mottled texture and brown to dark grayish brown matrix [38]. Thin clay lines most of the voids, resulting in a low permeability zone. The underlying “C” horizon is also clay-rich, dense, and dull reddish-brown to grayish-brown with rare mottling. The detailed soil horizon characteristics are described by Nowland and MacDougall [38].

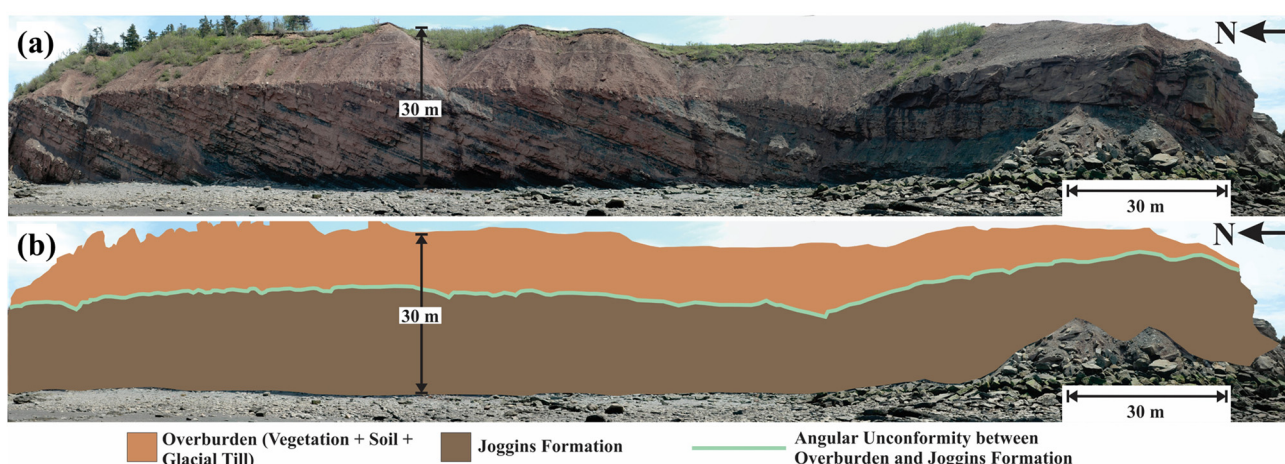


Figure 2. (a) An uninterpreted photograph of a section of the Joggins Formation showing the promontory on the left known as Coal Mine Point. (b) The same photograph as the top, except with some simple interpretation. The orange at the top indicates the portion known as overburden composed of vegetation, soil, and primarily glacial till. The brown area below the orange is the Joggins Formation. The green line between the two areas indicates the location of the well-defined angular unconformity.

Glacial till is defined as a mass of unsorted debris deposited by a glacier and consisting of grain sizes ranging from boulders to clay [40]. The glacial till on which these soil horizons were formed is a grayish, silty clay loam that originated from the fine-grained grey and red sandstones, shales and

mudstones of the Carboniferous coal measure beds [38]. A more recent study by Stea and Finck [41] names the till in this location as the Joggins Till. It is described as being a sandy silt that is dark yellowish-brown in colour with clasts composed of grey sandstones, shales, mudstones, and minor red sandstones and shales, limestone and coal [41].

3.2. *Bedrock geology*

The Maritimes Basin is comprised of ten onshore/offshore subbasins, of which the Cumberland Subbasin is one (Figure 3). It hosts numerous, well-known coal deposits, of which numerous seams and their associated mine workings are visible from the intertidal zone. The Joggins Formation is part of the Cumberland Group and with the Mabou Group forms a continuous 14.7 km long outcrop (Figure 4) along the coast of Chignecto Bay [24]. At approximately 4500 km², the Cumberland Subbasin is a fault-bounded depocenter containing some 7000 m of Late Devonian to Early Permian sediment (e.g., [42,43]). The subbasin occurs over areas of northwestern Nova Scotia and to a minor extent, regions of southern New Brunswick. It is positioned to the south by the Cobequid Mountains, to the west by the Caledonian Highlands and Westmorland Uplift, and to the east by the Antigonish Highlands (e.g., [43,44]). It is suggested by Browne and Plint [45] that the subbasin margins are comprised to the south by the North Fault, to the north by the Caledonia-Dorchester fault system, and to the west by the Harvey-Hopewell Fault. The northwestern basin margins, as suggested by Martel [46] are characterized by a laterally trending basal horst along the Hastings Fault.

A sequence of synclines occur in the basin, with the more significant examples being the Amherst, Athol, Scotsburn, Tatamagouche, and Wallace, in addition to a couple diapirism-related anticlines known as the Claremont-Malagash and Minudie, both being encircled by the aforementioned synclinal sequence [44]. According to Ryan and Boehner [44] the Cumberland Subbasin structural elements are correlated with basin growth features and include major synclines as well as growth and strike-slip faults. Those structural elements are either unrelated to or are indirectly related to salt tectonics and their related salt structures such as diapiric anticlines, diapirs, domes, and folds/faults related to salt movement [44]. The Cumberland Subbasin is considered a salt-withdrawal basin with both the slump features and movement of salt occurring concurrently with basin deposition.

The Joggins Formation has been interpreted to contain three stratigraphic facies; a well-drained floodplain facies that includes reddish siltstone, mudstone and sandstone with minor greyish mudstone, rare coal and limestone beds; a poorly-drained floodplain facies comprised of interbedded deposits of sand-poor and sand-rich beds, green/grey mudstone associated with coal, carbonaceous shale, and minor limestone; and an open-water facies (marine deposits) of sandstones and siltstones with thin limestone [22]. The strata dip to the south at approximately 21°.



Figure 3. Map showing the extent of the onshore and offshore regional Maritimes Basin extent. The Cumberland Subbasin is also included in the Maritimes Basin, but has been separately highlighted. The three major fault zones are as follows: CCFZ, Cobequid-Chedabucto Fault Zone; CFZ, Cabot Fault Zone; and HFZ, Hollow Fault Zone (modified from [47–50]). The acronym “PEI” stands for Prince Edward Island.

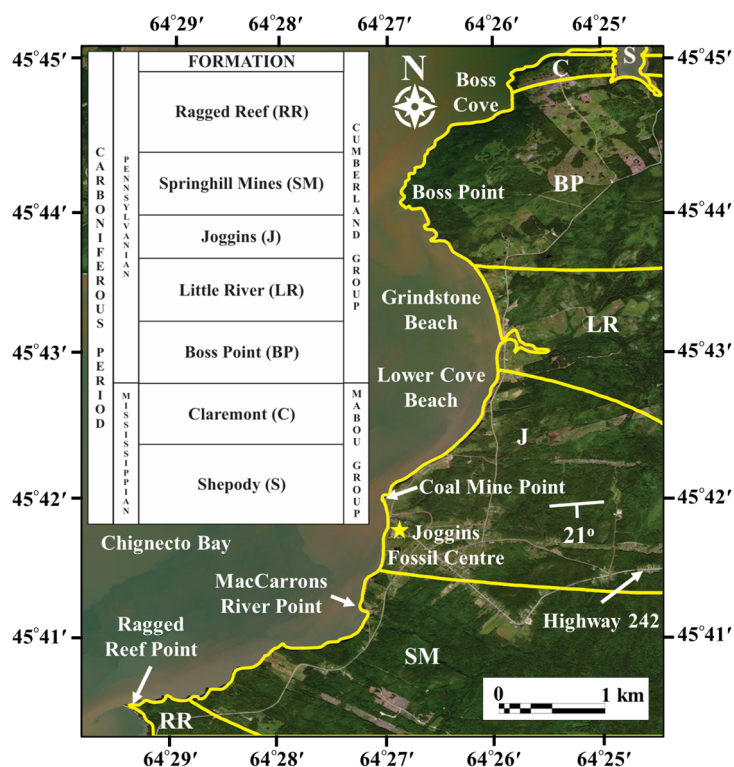


Figure 4. Plan view showing the Carboniferous Joggins Fossil Cliffs geology (modified from [24,37]). The stratigraphic column shows the geological formations with their relative ages. The formations, from both the Cumberland Group and Mabou Group, make up the conformable 14.7 km of strata coastline that is UNESCO recognized.

4. Equipment and methods

To achieve the research objectives of this study, a GPR and RTK DGPS system was used. To assist with GPR interpretation, data gathering was paired with an RTK DGPS to precisely georeference the GPR data. The Joggins Formation outcrop along the shoreline also provides a valuable 2-D view, while the GPR attempts to add the 3rd dimension. The outcrop study of the Joggins Formation helps to characterize and confirm the sedimentology and the internal architecture of the fluvial outcrop, particularly at smaller scales, which the GPR imaging is unable to resolve.

A Sensors and Software Incorporated pulseEKKO Pro SmartCart GPR system (Figure 5) was used for this study and supplied by the Dalhousie University Basin and Reservoir Laboratory. The cart is highly durable and has 4-wheels to provide the rapid and continuous collection of data in open areas. The cart is a self-contained system that includes the GPS rover receiver, transmitting and receiving antennae, digital video logging screen, and power supplies for the screen and antennae. The triggering method for the GPR survey is the built-in odometer. The transmitting and receiving antennae were oriented perpendicular to the line profile direction. The 50 MHz antennae with the standard transmitter/receiver configuration and a separation of 1.0 m was used for all lines. It was chosen because the specifications suggested a depth of penetration and resolution sufficient for Joggins Formation imaging. The 50 MHz antennae have a length of 2 m and a nominal spatial resolution length of at most 0.5 m. The step size is 0.1 m, the time window is 400 ns and there are 250 points per trace. The sampling interval is 1600 picoseconds (ps). The transmitter pulsar voltage is 1000 volts. The assumed velocity was 0.100 m/ns, which is between the value for wet clay and dry clay. The imaging of the Joggins Formation is captured to a depth of approximately 300 ns two-way travel time (TWT), corresponding to a depth of roughly 17.0 m. Setup parameters are listed in Table 1.

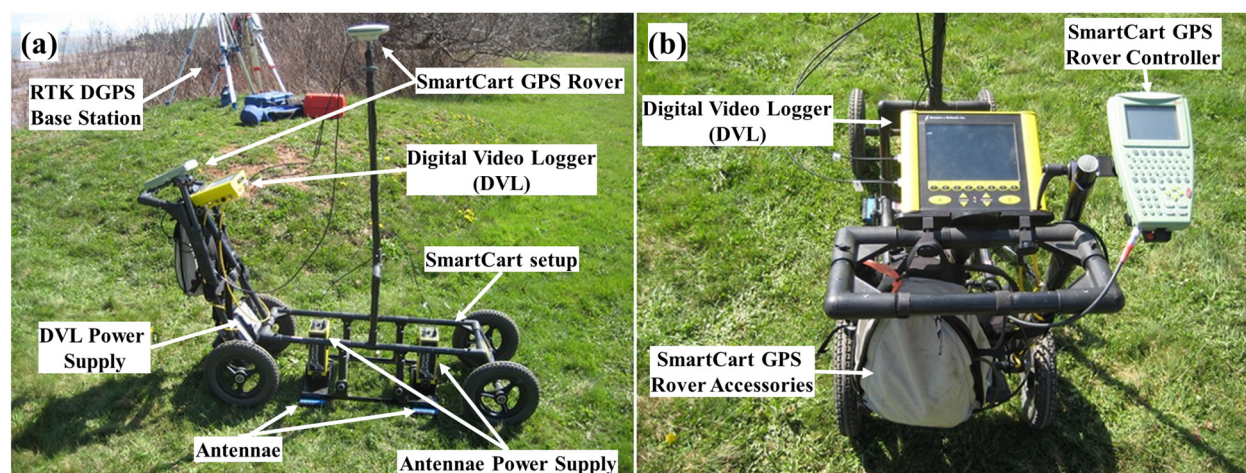


Figure 5. (a) The typical sideview of the GPR SmartCart setup with many of the features labelled. (b) The view from the operator's position looking at the GPR SmartCart. The operator has a clear view of the digital video logger (DVL) and the RTK DGPS rover controller. Note: the images show the setup with the 200 MHz antennae and not the 50 MHz antennae used for data collection.

The GPR system was paired with a RTK DGPS to provide a fully georeferenced group of survey lines with positional accuracy of approximately ± 2 cm [17]. The survey incorporated a Leica GPS1200+ Series High Performance Global Navigation Satellite System (GNSS) to apply differential corrections and broadcast accurate location data to the rover receiver. The GPS system consisted of a base station and a transmission antenna used to transmit corrections from the base station to the rover receiver in real-time (Figure 6). The rover receiver was mounted to the midpoint of the GPR cart. The base station was placed over a drilled water well with established surveyed coordinates (UTM Zone 20T; Easting = 387,098.72; Northing = 5,061,126.31; Elevation = 26.453 m) at the rear (water side) of the Joggins Fossil Cliffs Centre. As the GPR cart is pushed along a survey line, the rover receiver acquires GPS coordinates and the wander or drift that is recorded by the base station is subtracted in real-time from the coordinates recorded by the GPR cart. The corrected points are then recorded into the radargram.

Table 1. Summary table of GPR system setup parameters.

	Value/Description
<i>GPR Parameters</i>	
Antenna Frequency	50.0 MHz
Antenna Separation	1.000 m
Assumed Velocity	0.100 m/ns 0.328 ft/ns
Time Window	400.00 ns
Number of Points	250
Sample Interval	1.60 ns
System Stacking	32
Pulsar Settings	Auto PRO
<i>Survey Parameters</i>	
Start Position	0.00 m
Antenna Step Size	0.100 m
Position Units	Metric
Survey Type	Reflection
<i>Acquisition Control Parameters</i>	
Triggering Method	Odometer
Trace Delay	0.0 sec
Odometer Calibration	1045.75 forward
Beeper Active	None
Data Storage	Removable
GPS Usage	Every Trace
GPS Baud Rate	19200
GPS Transfer Bits	1s 8d N
GPS End String	\$GPRMC
<i>Display Parameters</i>	
Trace Type	Grey Scale
Trace Spacing	8 pixels
Gain Type Applied	SEC

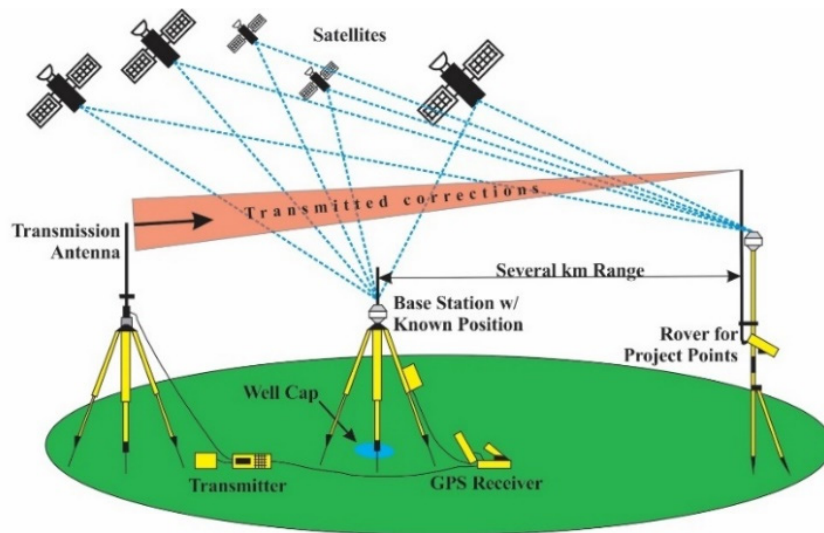


Figure 6. Sketch of the global positioning system equipment used to provide a fully georeferenced ground-penetrating radar data set (modified from [17,48]). The base station was assembled over a drilled water well with known coordinates. The transmission antenna was placed adjacent to the base station. The rover was mounted on the GPR SmartCart for providing survey line locational coordinates.

The processing workflow follows three main tasks; the first being the selection of an acceptable GPR data processing workflow; the second being the selection of the appropriate parameters and inputs for each processing step, where required (the dewow filter does not have any inputs, it is simply applied or not applied); and finally, the observation of end results for each processing step and the correction of any issues caused by an incorrect parameter [51]. EKKO_Project™ software was used for editing, processing, and viewing the GPR data. The software was developed by Sensors and Software Incorporated and is a professional “software version that allows for data plotting, editing and full processing routines including spatial and temporal filters, migration, instantaneous attributes, amplitude spectra, CMP velocity analysis and more.” All GPR data were post-processed. Processing was performed using iterations paired with descriptions of how and when each processing technique should be applied. Processes were applied individually and in conjunction with other processes until the radargram was sufficient for interpretation.

The GPS data was collected concurrently with the GPR data on the Sensors and Software Digital Video Logger (DVL) and was added to the GPR data using the file that recorded GPS positions at regular trace intervals. The GPS data was stored as the GGA (Global Positioning System Fix Data) format, which is a standard format recognized by the National Marine Electronics Association. The GPS data was converted to UTM coordinates and the step-size re-calculated. Topographic correction of the GPR data along the survey lines was performed using the EKKO_Project™ software. The topographic variation along the survey areas is shown on the inset elevation profile plot in Figure 7a.

Signal saturation correction or dewow is a type of time filter and was applied to each trace for the removal of the initial DC component and low-frequency, slowly decaying “wow” [52,53]. This is caused by the arrival of early waves, dynamic range limitations on instrumentation, and/or inductive

coupling effects and becomes superimposed on the high frequency reflections [52,53]. It is typically almost always applied and is usually the first process applied.

To compensate for the spreading and attenuation of the propagating wave front, the Spreading and Exponential Compensation (SEC) gain was used to apply the exponential gain (approximately $1/r^2$) that compensates for the spreading and attenuation of the propagating wave front. The input parameters necessary for this gain are an attenuation value for the substrate, a beginning value to be added to the exponential gain function and a maximum value for the gain. The average time-amplitude plot for each trace was examined both before and after the application of the gain to ensure it was properly applied as described by Annan [54]. Each line had unique attenuation, start and maximum values. The values for attenuation ranged between 2.08 and 5.31 dB/m with an average of 3.63 dB/m. The start gain value ranged from 0.62 to 1.44 with an average of 0.92. The maximum gain value applied ranged from 32 to 222 with an average of 123.79.

5. Survey area

A localized GPR survey was carried out along 3 gravel roads and one grassy field over the Joggins Formation. The four areas are Hardscrabble Road, Main Street, a grassy area adjacent to Main Street, and Mitchell Street (Figure 8). The GPR survey conducted on Hardscrabble Road consisted of 31 lines (lines 09–39) between elevations ranging from 17 to 48 m above sea level for a total distance of approximately 2500 m. A representative image of Hardscrabble Road can be seen in Figure 8a. The GPR survey conducted on Mitchell Street consisted of 1 line (line 51) between elevations ranging from 31 to 43 m above sea level for a total distance of approximately 434 m. A representative image of Mitchell Street can be seen in Figure 8b. The GPR survey conducted on the grassy field adjacent to Main Street consisted of 5 lines (lines 45–50) between elevations ranging from 24 to 27 m above sea level for a total distance of approximately 236 m. A representative image of the grassy area adjacent to Main Street can be seen in Figure 8c. The GPR survey conducted on Main Street consisted of 5 lines (lines 40–44) between elevations ranging from 19 to 31 m above sea level for a total distance of approximately 307 m. A representative image of Main Street can be seen in Figure 8d. In summary, the GPR survey consisted of a total of 42 lines over the Joggins Formation between elevations from 16.97 m to 47.47 m above sea level for a total distance of approximately 3500 m (Figure 8a; Table 2). The roads are primarily non-linear, so the survey was completed using numerous short straight-line segments.

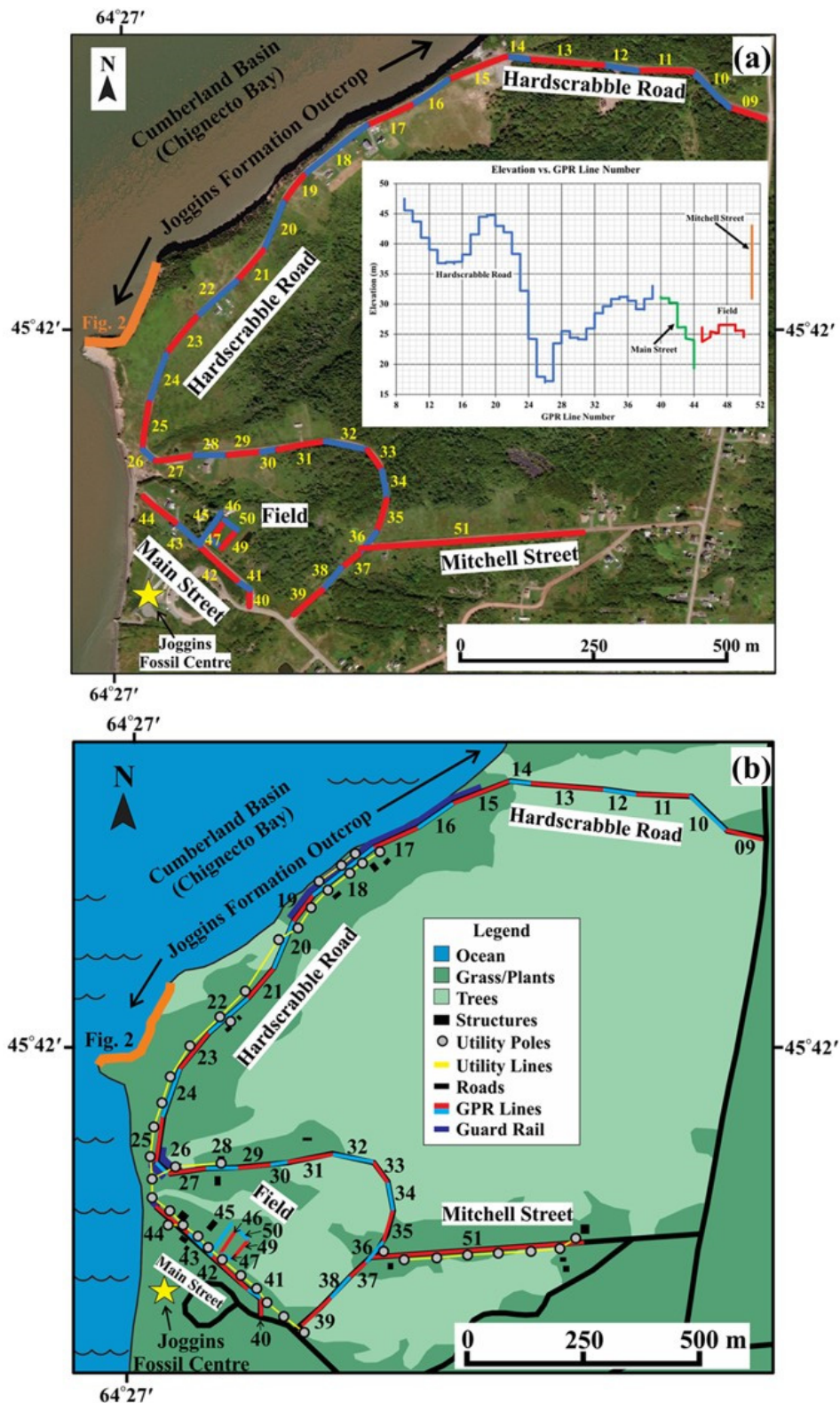


Figure 7. (a) Satellite image of the study area showing GPR line locations with contrasting blue and red lines (basemap from [37]). The inset graph plots the survey elevation profile. (b) Plan view sketch of the study area showing the GPR lines in relation to surficial features (basemap from [37]).

The GPR survey areas are sparsely populated; however, there are an abundance of surficial features, both human-made and natural, that may have varying effects on the quality of the GPR data collected. Many of the surficial features and objects that occur adjacent to or in the vicinity of GPR data collection are shown in Figure 7b. Residential dwellings are generally well-spread out, but are located in certain areas along Hardscrabble Road, Main Street, and Mitchell Street. Along with these dwellings is the associated infrastructure, mainly utility poles and power lines, which do occur in abundance adjacent to the three road surfaces surveyed. The infrastructure also includes steel guard rails with wooden posts along the road areas that closely border the cliff edge. Areas of vegetation (e.g., grass, plants, and trees) are also located along the flanks of the roads where the GPR surveys were completed on. Due to the variation in surficial features along the GPR survey lines, it may be possible to look for subtle changes in the reflection profiles and correlate the response to a particular feature.

Table 2. A summary of the 42 GPR lines collected at Joggins.

Line	Line Length (m)	# Traces	Min Elev. (m)	Max Elev. (m)
Line09 ¹	71.5	144.0	45.55	47.47
Line10 ¹	100.5	202.0	43.69	45.51
Line11 ¹	107.5	216.0	41.01	43.68
Line12 ¹	67.5	136.0	39.02	40.98
Line13 ¹	145.5	292.0	36.79	38.99
Line14 ¹	44.0	89.0	36.73	36.96
Line15 ¹	120.5	242.0	36.69	37.01
Line16 ¹	87.0	175.0	37.03	38.22
Line17 ¹	95.0	191.0	38.22	41.56
Line18 ¹	156.5	314.0	41.57	44.49
Line19 ¹	65.0	131.0	44.49	44.85
Line20 ¹	102.0	205.0	42.95	44.74
Line21 ¹	79.0	159.0	41.93	42.97
Line22 ¹	105.0	211.0	38.33	41.92
Line23 ¹	93.0	187.0	32.20	38.31
Line24 ¹	100.5	202.0	24.23	32.18
Line25 ¹	92.0	185.0	17.93	24.18
Line26 ¹	34.0	69.0	16.97	17.90
Line27 ¹	77.0	155.0	17.20	23.45
Line28 ¹	64.5	130.0	23.47	25.48
Line29 ¹	65.5	132.0	24.38	25.48
Line30 ¹	33.0	67.0	24.12	24.40
Line31 ¹	93.0	187.0	24.09	25.93
Line32 ¹	84.0	169.0	25.94	28.48
Line33 ¹	49.5	100.0	28.45	29.62
Line34 ¹	56.5	114.0	29.61	30.85
Line35 ¹	66.5	134.0	30.79	31.19
Line36 ¹	54.5	110.0	30.52	31.31

Continued on next page

Line	Line Length (m)	# Traces	Min Elev. (m)	Max Elev. (m)
Line37 ¹	43.5	88.0	29.14	30.53
Line38 ¹	57.0	115.0	29.06	30.85
Line39 ¹	73.5	148.0	30.88	33.00
Line40 ²	34.5	70.0	30.94	31.18
Line41 ²	31.0	63.0	30.20	30.97
Line42 ²	98.0	197.0	26.11	30.20
Line43 ²	62.0	125.0	24.27	26.17
Line44 ²	81.0	163.0	19.32	24.02
Line45 ³	72.5	146.0	23.76	26.09
Line46 ³	53.0	107.0	24.52	25.43
Line47 ³	33.5	68.0	25.14	26.51
Line49 ³	46.5	94.0	25.51	26.57
Line50 ³	30.5	62.0	24.50	25.60
Line51 ⁴	433.5	868.0	30.90	43.04

¹-lines collected on Hardscrabble Road;

²-lines collected on Main Street;

³-lines collected on a grassy area adjacent to Main Street;

⁴-line collected on Mitchell Street.

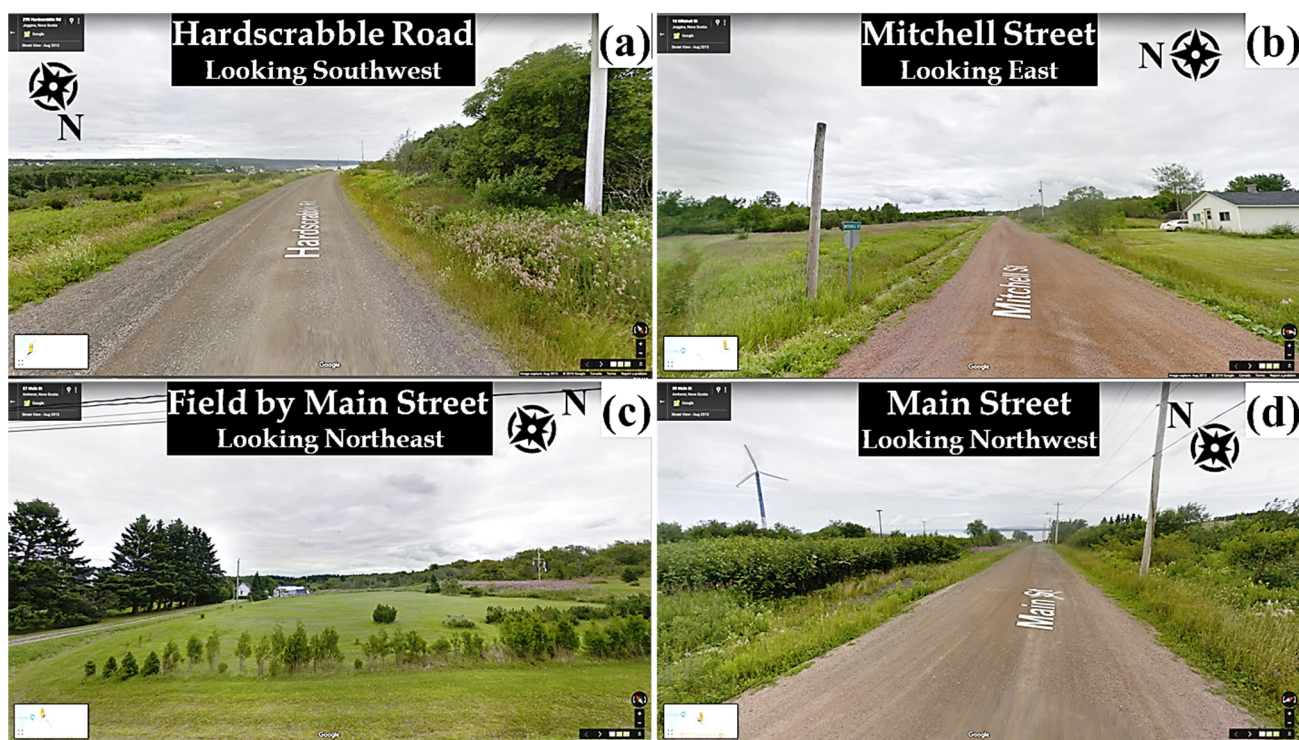


Figure 8. Representative images of the four areas on which GPR surveying was completed. The four areas over which GPR surveying was done includes (a) Hardscrabble Road, (b) Mitchell Street, (c) a grassy area adjacent to Main Street, and (d) Main Street [55].

6. Results

6.1. Processed radargrams

The completion of the GPR survey at Joggins, Nova Scotia resulted in 42 unique radargrams across three road surfaces (Hardscrabble Road, Main Street, and Mitchell Street) and a grassy area adjacent to Main Street. The 42 processed radargrams are displayed in Figure 9. All radargrams have an initial high amplitude, thick, horizontally continuous reflector. It always occurs at the top of the radargram and follows the topography of the individual survey line.

In addition, all radargrams display a second high amplitude, thick, primarily horizontally continuous reflector that is always below the primary top reflector. It too will generally follow the topography of the individual survey line, but can be discontinuous. Numerous radargrams contain high amplitude, sharp, concave downwards reflectors that have a consistent shape and are either overlapping or have a consistent spacing. In general, coherent reflectors are absent below approximately 6 to 8 m depth. The resulting reflectors that are visible in the radargrams are summarized in the following radar reflectors section and in Figure 10. In total, 13 radar reflectors are described and interpreted.

6.2. Radar reflectors

Selected results from four areas surveyed across the Joggins Formation are presented here. The variability in surficial features along the various surveys results in reflectors that can be correlated nicely to these features. A total of thirteen unique radar reflectors have been identified from the GPR data and are briefly summarized (Figure 10). RR1 is a high amplitude, thick reflection and is the first signal measured by the receiver and occurs in all 42 collected radargrams. It is continuous for the complete length of each radargram and is followed by a low amplitude signal. It follows the natural topography of the GPR survey line. There are no other features that occur with this reflector. RR2 is a high amplitude, thick reflection and is the second signal measured by the receiver and occurs in all 42 collected radargrams. It is typically continuous for the complete length of each radargram, although it can be discontinuous in several lines. It is followed by a low amplitude signal. It follows the natural topography of the GPR survey line. This reflector is affected by the subsurface and surficial features. Reflectors RR3 is characterized by a thin, high amplitude reflection, followed by a lower amplitude signal. This reflector occurs at approximately 8 m depth in the radargrams it occurs in, which is consistent with the approximate depth of the overburden in the area. The RR4 reflector is common throughout the radargrams. It is characterized by regularly spaced; high amplitude followed by low amplitude concave downwards reflectors. They have a consistent shape and are sharply outlined.

The RR5 reflector is also common throughout the radargrams. It is characterized by irregularly spaced; high amplitude followed by low amplitude concave downwards reflectors. They have a less consistent shape and are not as sharply outlined as the RR4 reflector. reflector RR6 is not common throughout the radargrams and is characterized by a break in the second thick, high amplitude reflector. The RR7 reflector is characterized by high amplitude, repeating, and parallel reflectors that reverberate throughout the radargram. The RR8 reflector is reflection-free. There are no coherent reflectors observed in the radargrams. RR9 is a thick, high amplitude, concave downwards reflection that only

appears to be visible in a couple of radargrams. It is associated with the high amplitude, thick, continuous reflector (RR2). RR10 is a high amplitude, thick, and discontinuous reflector that occurs below RR2. It displays an undulating profile and is only visible in a single radargram. RR11 is a continuous, upright, high/low amplitude reflector that mimics a teepee shape. It is very-well defined and sharp. It occurs in only five radargrams. RR12 is a vertical, mottled high and low amplitude reflector that is only visible in a single radargram. The features are not continuous throughout the whole radargram. RR13 is a small, near-surface, high amplitude reflector. It is concave downwards and sharp with a consistent shape. They are associated with RR2.

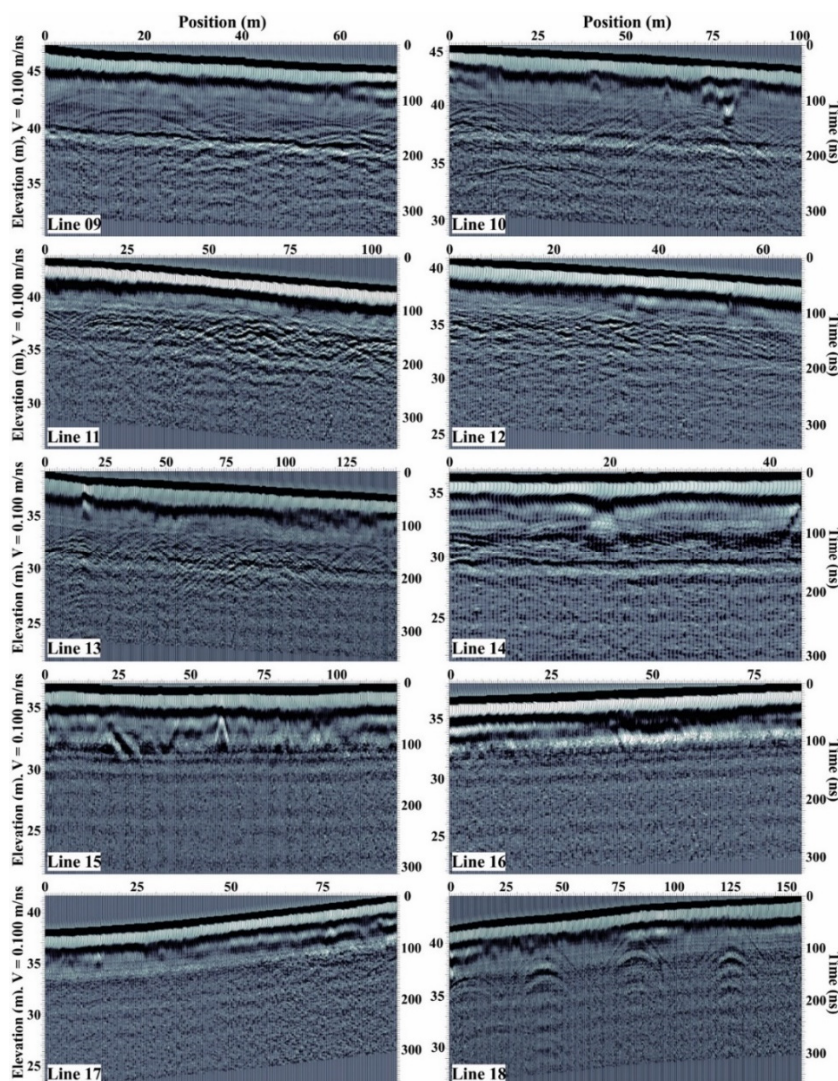


Figure 9. Radargrams for lines 09 to 18 inclusive with position on the upper abscissa, elevation on the left ordinate and time on the right ordinate. Radargrams for lines 19 to 28 inclusive with position on the upper abscissa, elevation on the left ordinate and time on the right ordinate. Radargrams for lines 29 to 38 inclusive with position on the upper abscissa, elevation on the left ordinate and time on the right ordinate. Radargrams for lines 39 to 51 inclusive with position on the upper abscissa, elevation on the left ordinate and time on the right ordinate.

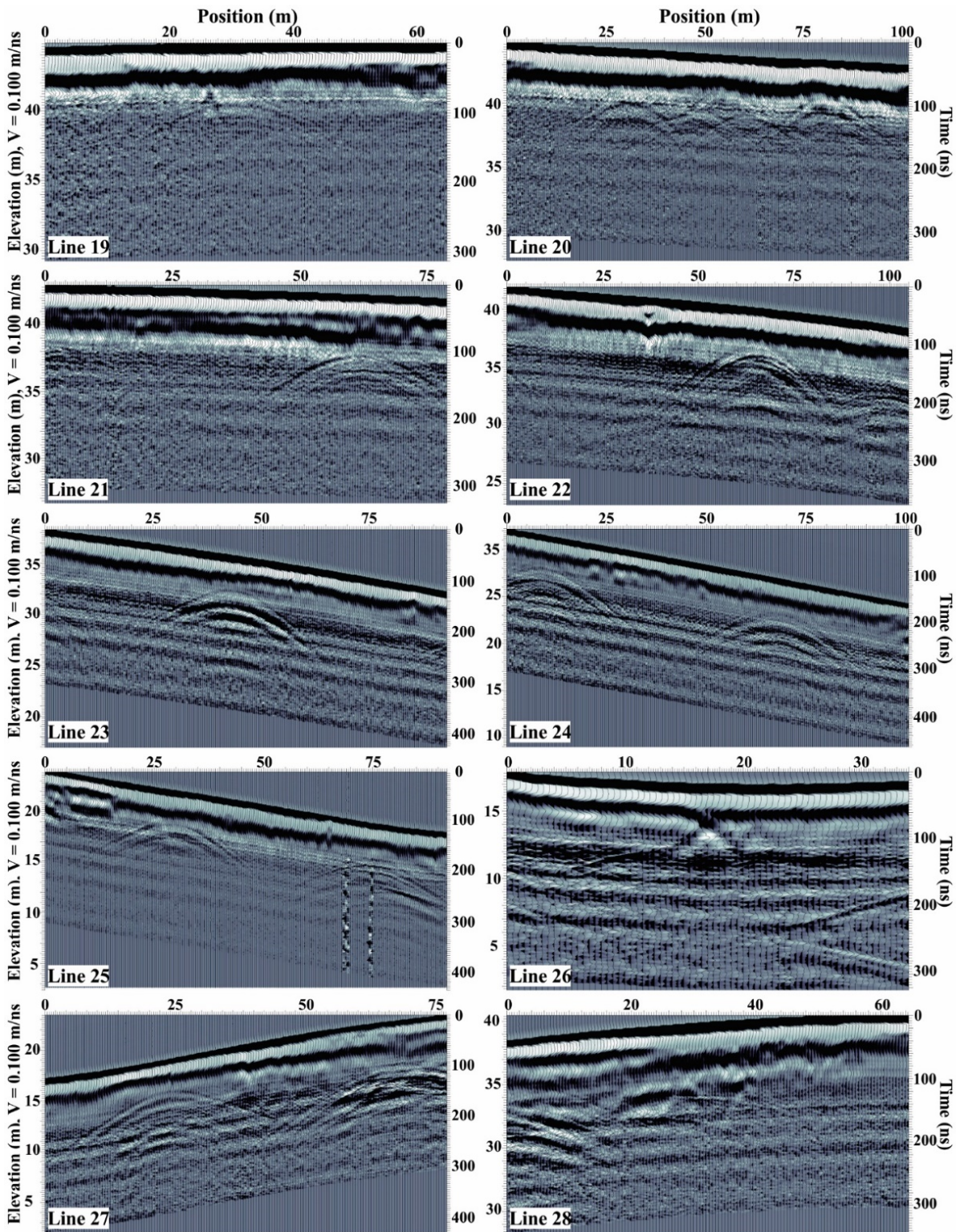


Figure 9. Continued.

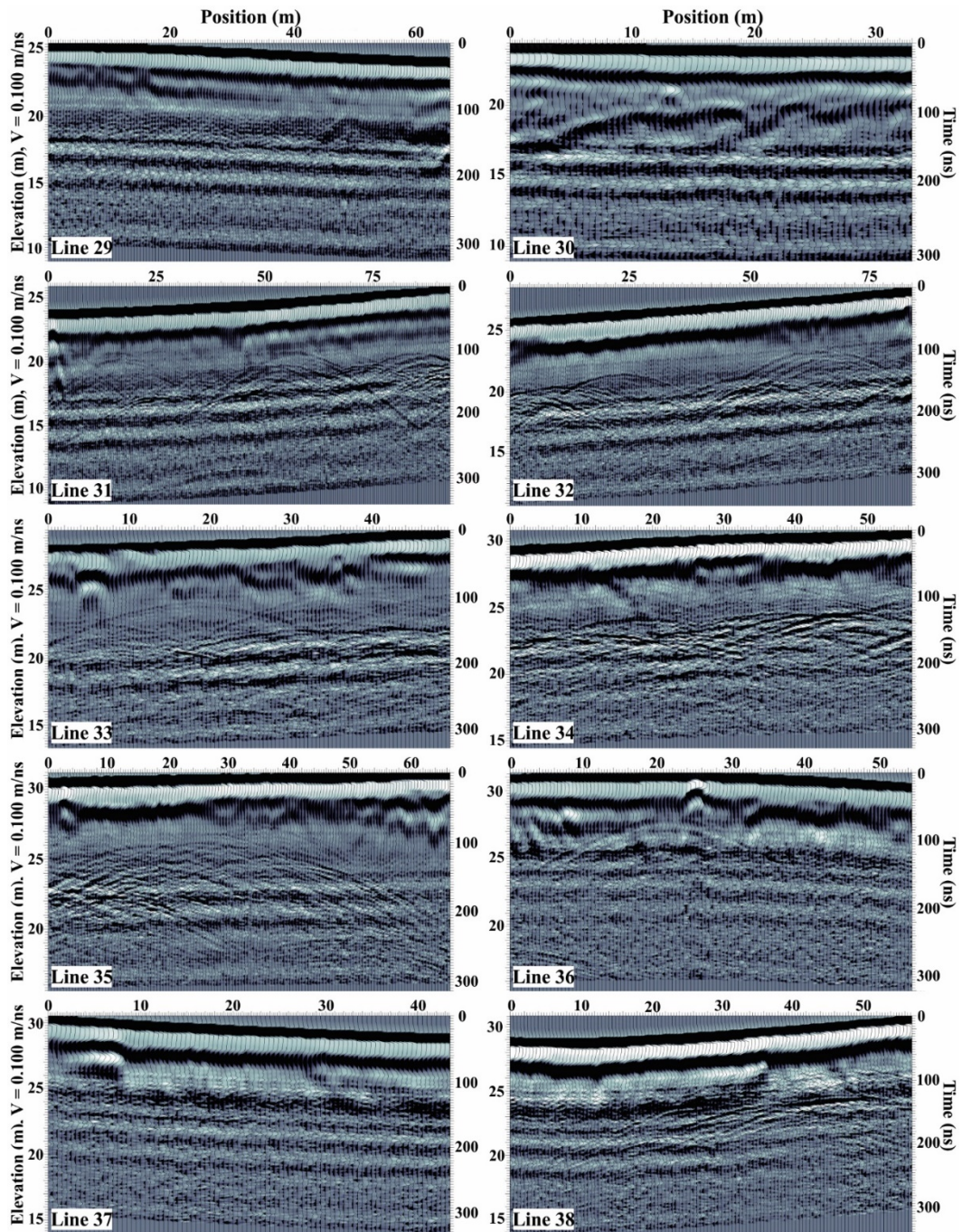


Figure 9. Continued.

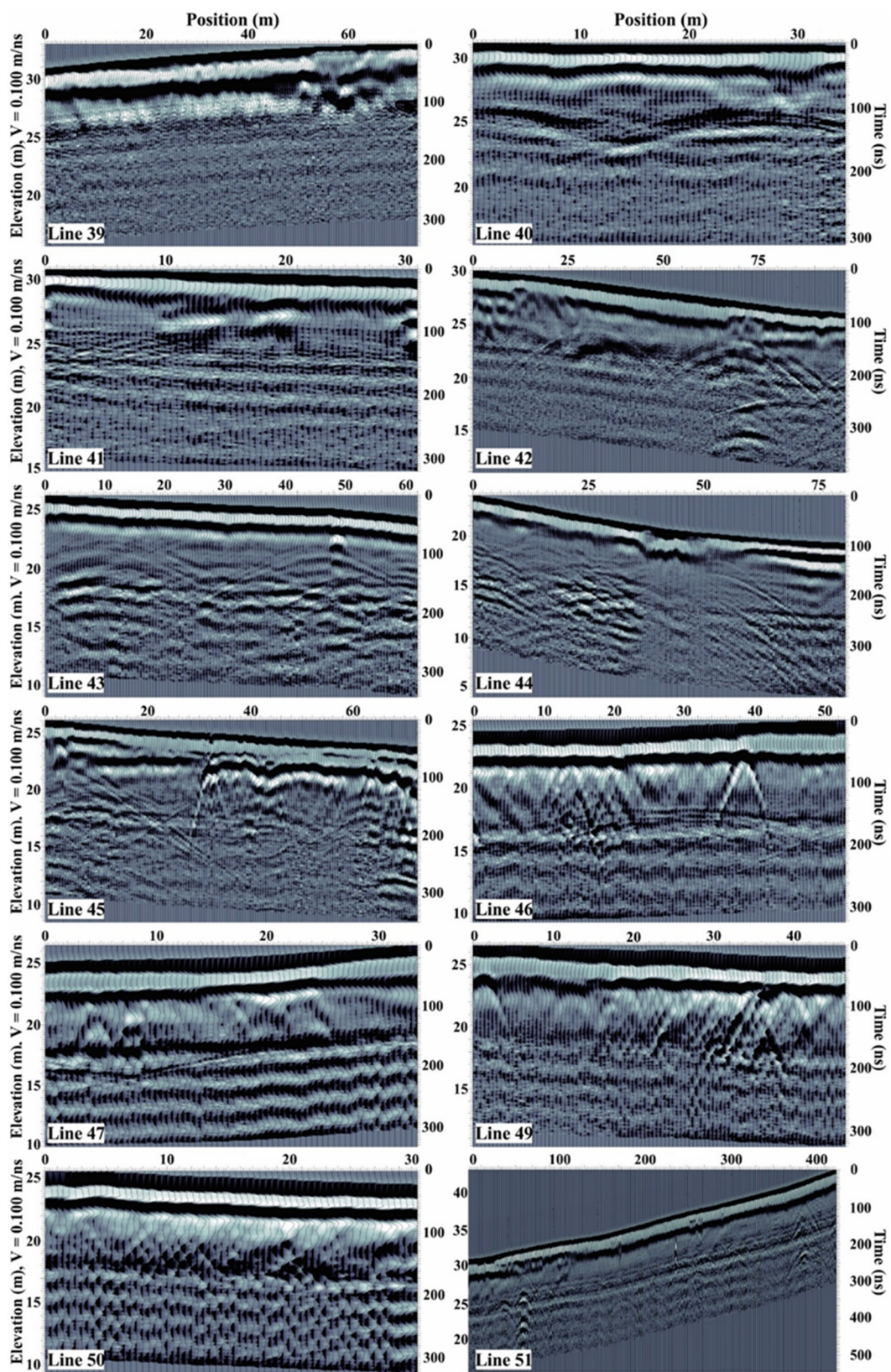


Figure 9. Continued.

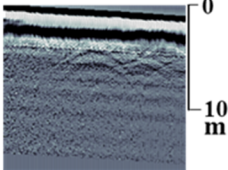
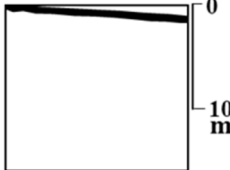
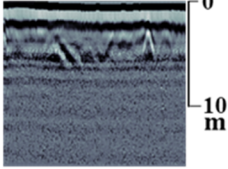
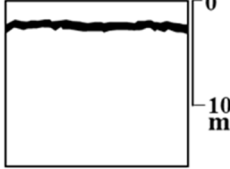
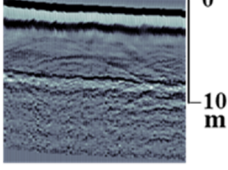
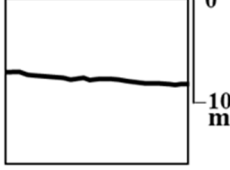
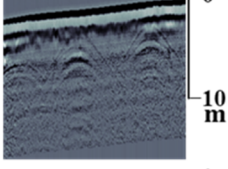
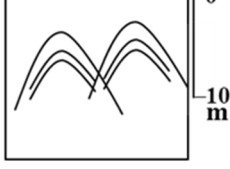
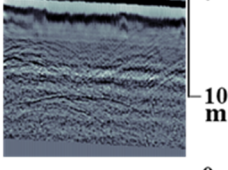

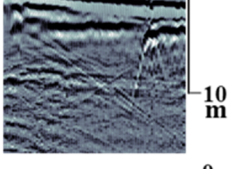
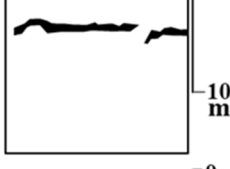
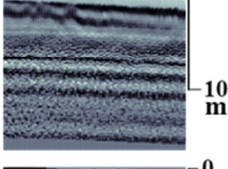

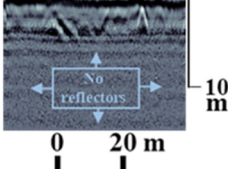
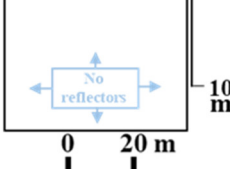
Radar Reflectors	GPR Example	GPR Interpretation	Associated Lines
RR1- High amplitude, thick, continuous reflector; always at top of profile			All (Hardscrabble Road, Main Street, grassy area off Main Street, and Mitchell Street)
RR2- High amplitude, thick, continuous reflector; always below primary top reflector			All (Hardscrabble Road, Main Street, grassy area off Main Street, and Mitchell Street)
RR3- High amplitude followed by low amplitude reflector; continuous; occurs at 6 to 8 m depth			9, 10, 11, 13, 14, 15, 29 (Hardscrabble Road); 51 (Mitchell Street)
RR4- Regularly spaced, high amplitude, sharp, concave downwards reflector; consistent shape			18, 19, 20, 21, 22, 23, 24, 25, 27, 36 (Hardscrabble Road); 42, 43, 44 (Main Street); 51 (Mitchell Street)
RR5- Irregularly spaced, high amplitude sharp, concave downwards reflector; inconsistent shape			9, 10, 11, 12, 13, 15, 20, 27, 31, 32, 33, 34, 35 (Hardscrabble Road); 51 (Mitchell Street)
RR6- Break in the high amplitude, thick, continuous reflector; always below primary top reflector			27, 39 (Hardscrabble Road); 45 (grassy area off Main Street)
RR7- High amplitude repeating reflector; reverberations			All (Hardscrabble Road, Main Street, grassy area off Main Street, and Mitchell Street)
RR8- Coherent reflectors are absent			All (Hardscrabble Road, Main Street, grassy area off Main Street, and Mitchell Street)

Figure 10. Radar reflectors identified in the 42 radargrams from the Joggins area. The radar reflectors and description, a GPR example from the data collected, the outline interpretation of that feature, and the associated lines the feature occurs in are shown.

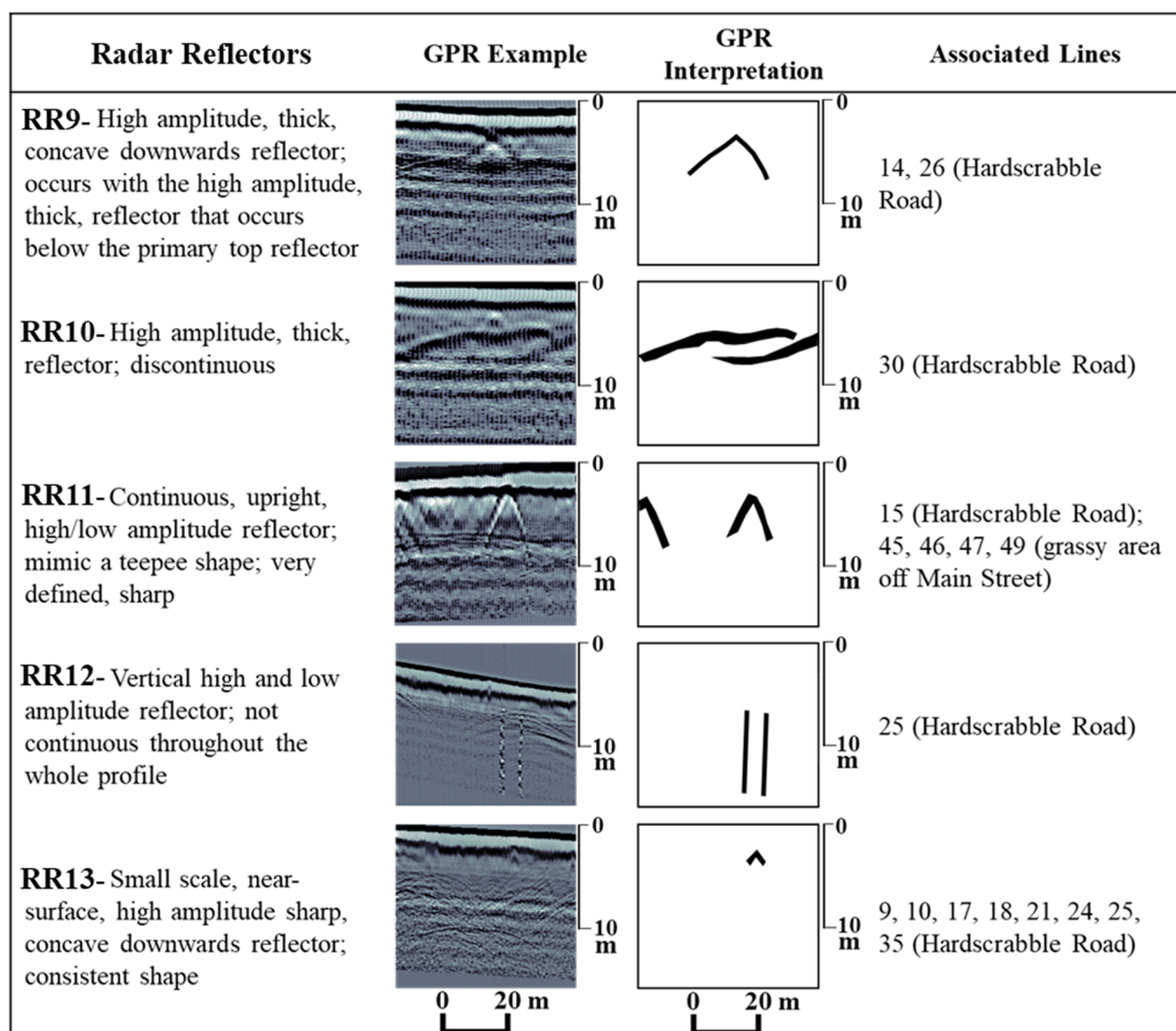


Figure 10. Continued.

7. Discussion

RR1 is defined as the direct air wave. This high amplitude reflection is the first signal measured by the receiver and occurs in all 42 collected radargrams. It is continuous for the complete length of each radargram and is followed by a low amplitude signal. Typical examples of this radar reflector can be seen in all radargrams, including radargrams 31 and 37 (Figure 11). Since the radargrams have all been georeferenced, the direct air wave follows the topography.

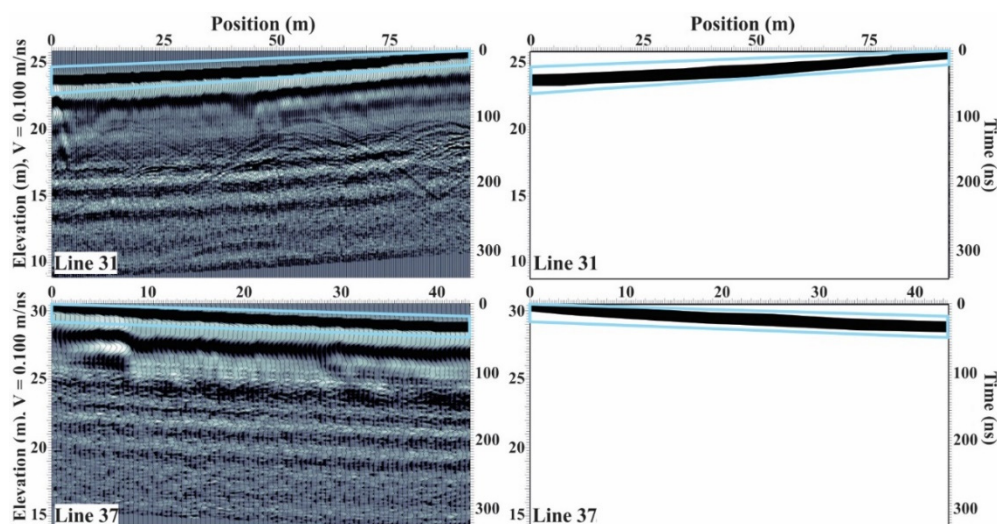


Figure 11. Uninterpreted radargram of line 31 and 37 on the left and interpreted radargram of line 31 and 37 on the right showing examples of radar reflector 1, which is interpreted to represent the direct air wave.

RR2 is defined as the direct ground wave. This high amplitude reflection is the second signal measured after the direct air wave and is also present in all 42 radargrams. The majority of the radargrams display a continuous direct ground wave, except for lines 27, 39, and 45 in which they are discontinuous. Typical examples of this radar reflector can be seen in all radargrams, including radargrams 31 and 43 (Figure 12). The undulating nature of the ground wave highlights the small topographic changes that occur over the lengths of each GPR line segment.

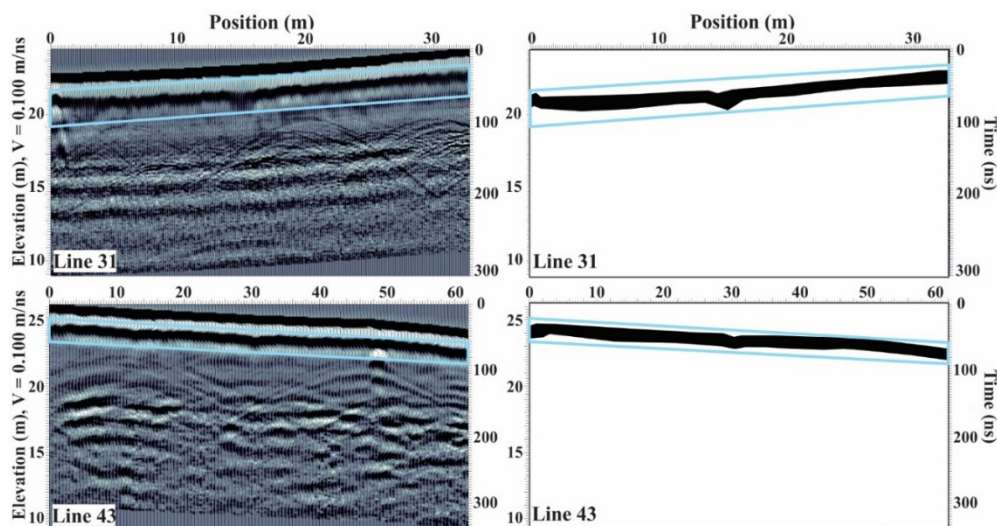


Figure 12. Uninterpreted radargram of line 31 and 43 on the left and interpreted radargram of line 30 and 43 on the right showing examples of radar reflector 2, which is interpreted to represent the direct ground wave.

RR3 is interpreted to represent the angular unconformity contact between the Carboniferous-aged Joggins Formation and the overlying Quaternary-aged glacial till and soil cover. The sharpness of the contact as well as the depth it is occurring at (6 to 8 m) are the main reasons for this interpretation. Curiously though, this reflector is not present in all radargrams, even though all survey lines were completed on top of overburden overlying the Joggins Formation. Examples of this radar reflector can be seen in several radargrams, including radargrams 09 and 13 (Figure 13).

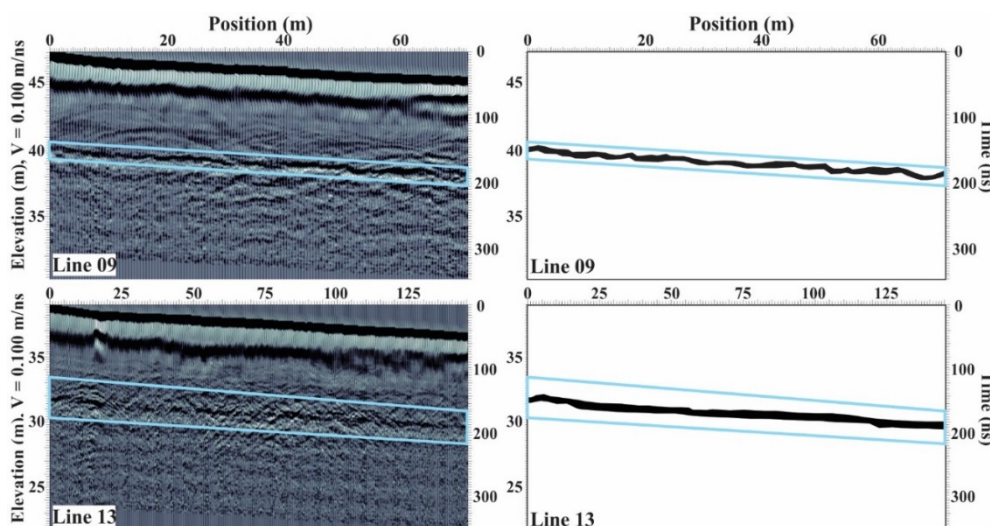


Figure 13. Uninterpreted radargram of line 09 and 13 on the left and interpreted radargram of line 09 and 13 on the right showing examples of radar reflector 3, which is interpreted to represent the angular unconformity contact.

The RR4 reflector correlates to utility poles that are erected at certain locations adjacent to the road surfaces. Several radargrams were recorded along road surfaces that have regularly spaced wooden utility poles located less than 10 m from the centerline of the road. The data from these lines show regularly spaced, clear, and sharp, concave downwards reflectors whose locations match those of the utility poles along the survey lines. Typical examples of this radar reflector can be seen in several radargrams, including radargrams 18 and 23 (Figure 14).

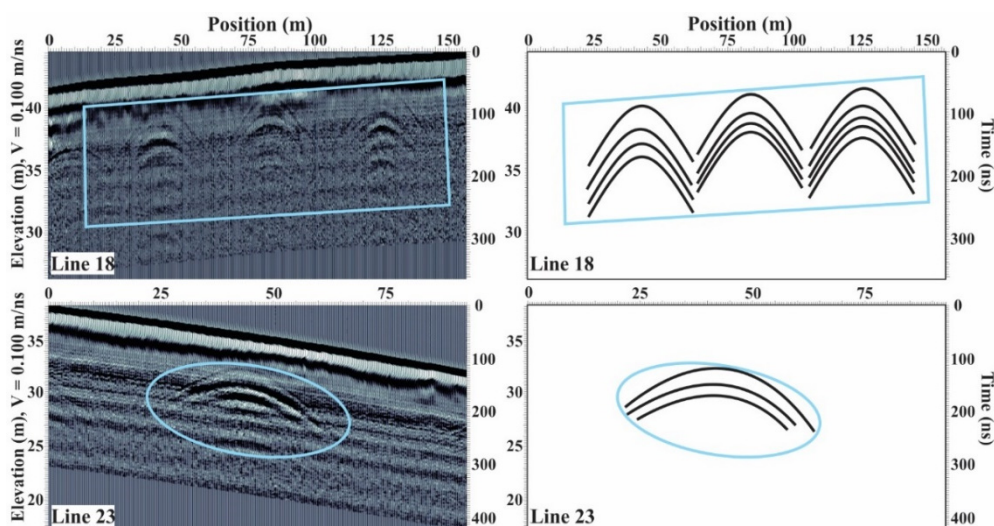


Figure 14. Uninterpreted radargram of line 18 and 23 on the left and interpreted radargram of line 18 and 23 on the right showing examples of radar reflector 4, which is interpreted to represent the utility poles adjacent to the road surfaces.

The RR5 reflector is also composed of concave downwards reflectors. However, these reflectors are noticeably different when compared to the utility poles described by RR4. Through careful examination of the radargrams, it was determined that RR5 represent trees. In contrast to the regularly spaced utility poles giving regular and clear diffraction hyperbolae, trees on the other hand produce hyperbolae that are randomly occurring and are overlapping. This theory was tested by viewing the GPR lines that did not have power line infrastructure located next to the road surface, but did have abundant, randomly occurring trees. Representative examples of this radar reflector can be seen in radargrams 10 and 32 (Figure 15).

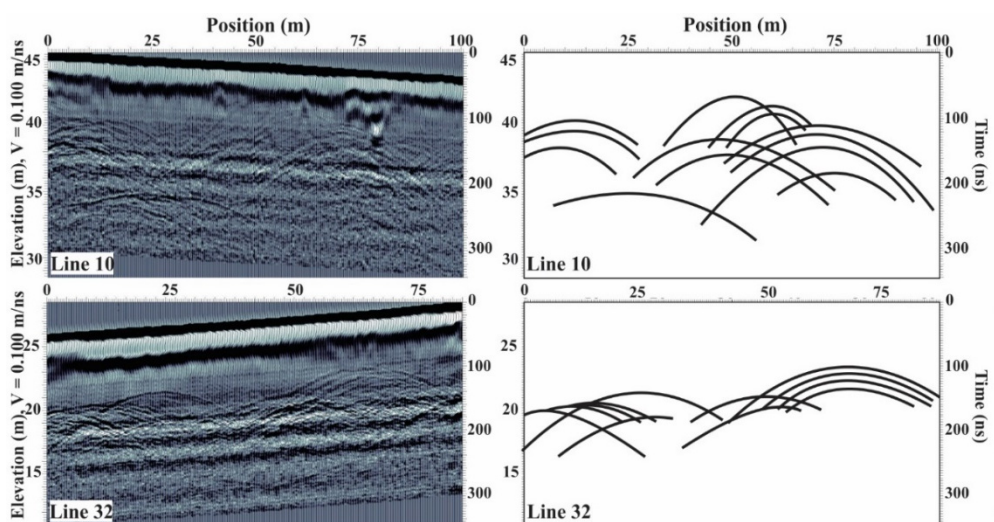


Figure 15. Uninterpreted radargram of line 10 and 32 on the left and interpreted radargram of line 10 and 32 on the right showing examples of radar reflector 5, which is interpreted to represent the reflections caused by trees adjacent to the road surfaces.

The RR6 reflector is rarely observed in the radargrams. The survey lines where this reflector becomes discontinuous are also the areas where the GPR has passed beneath a power line. It can therefore be surmised that overhead power lines can cause a brief break in the direct ground wave. Typical examples of this radar reflector can be seen in radargrams 27 and 39 (Figure 16).

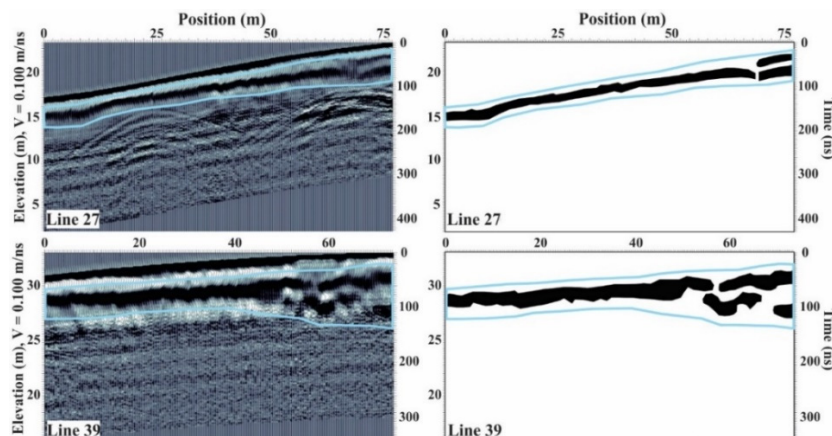


Figure 16. Uninterpreted radargram of line 27 and 39 on the left and interpreted radargram of line 27 and 39 on the right showing examples of radar reflector 6, which shows the direct ground wave becoming discontinuous when the GPR survey passes beneath a power line.

The RR7 reflector represent multiples or reverberations of the electromagnetic energy, probably as a result of the clay-rich soil and glacial till. These types of reflectors occur throughout all the radargrams, although they may be subtle. Representative examples of this radar reflector are shown in radargrams 29 and 31 (Figure 17).

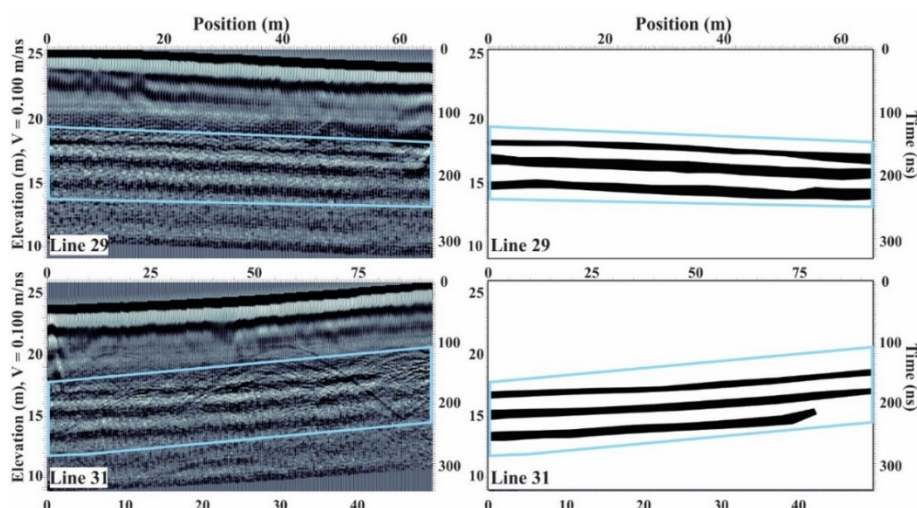


Figure 17. Uninterpreted radargram of line 29 and 31 on the left and interpreted radargram of line 29 and 31 on the right showing examples of radar reflector 7, which shows multiples or reverberations within the data.

We interpret the RR8 reflector as areas where the GPR signal has been attenuated. This typically signifies either a lithological unit that is massive and homogenous, the presence of dissolved minerals in groundwater with highly conductive properties, and/or the presence of clay-rich sediments (e.g., [56,57]). In this study, it was determined that the attenuation was caused by the overlying clay-rich glacial till and soil. This reflector makes up the majority of all radargrams and is widespread among all 42 radargrams, indicating that at least locally, the clay-rich glacial till and soil are probably present. Typical examples of the attenuated signal can be seen in radargrams 19 and 20 (Figure 18).

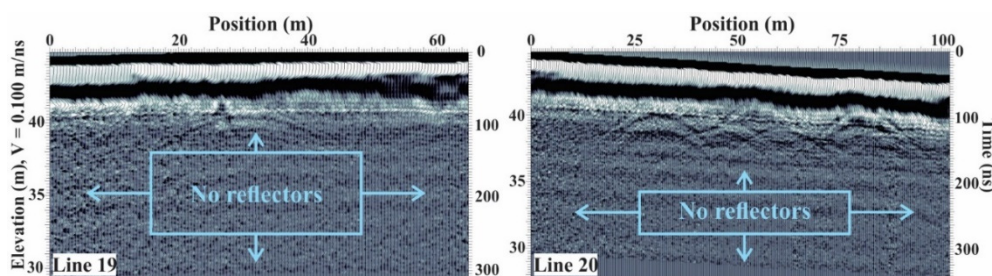


Figure 18. Uninterpreted radargrams of lines 19 and 20 showing examples of radar reflector 8, which show examples of the attenuated GPR signals.

The RR9 reflector is rarely observed in the radargrams but is interpreted to represent culverts that are installed beneath the road surface. Typical examples of this radar reflector can be observed in radargrams 14 and 26 (Figure 19). It was not observed if a culvert actually exists beneath the line 14 road segment of Hardscrabble Road; however, one was observed beneath the segment of Hardscrabble Road traversed by line 26.

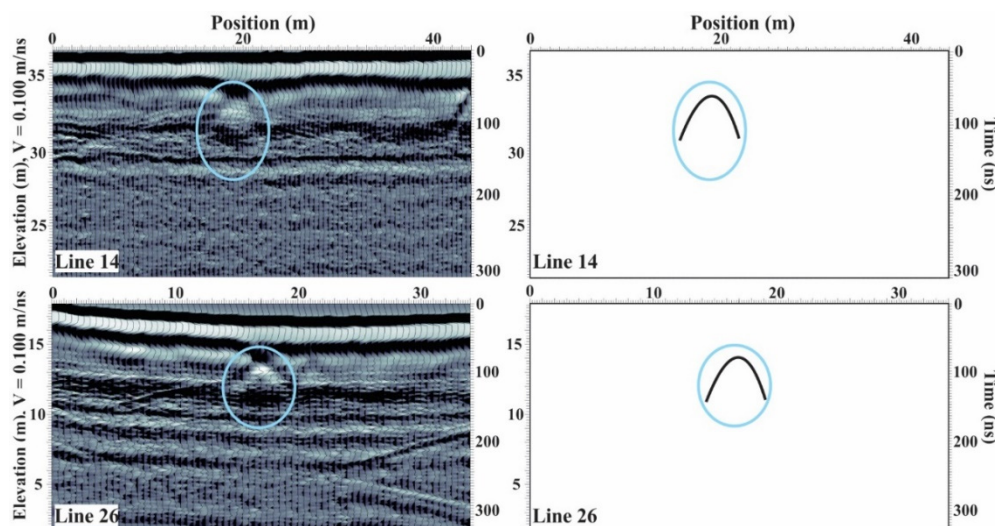


Figure 19. Uninterpreted radargram of line 14 and 26 on the left and interpreted radargram of line 14 and 26 on the right showing examples of radar reflector 9, which is interpreted to represent culverts beneath the roadway.

RR10 is interpreted to represent the undulating angular unconformity contact between the Carboniferous-aged Joggins Formation and the overlying Quaternary-aged glacial till and soil cover. The sharpness of the contact as well as the depth it is occurring at (6 to 8 m) are the main reasons for this interpretation. The lone example of this radar reflector can be seen in radargram 30 (Figure 20).

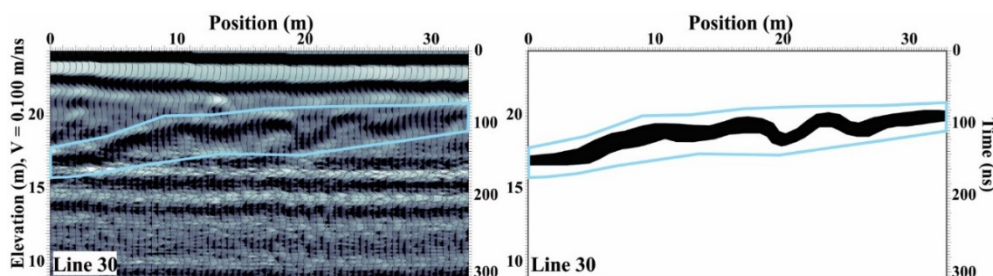


Figure 20. Uninterpreted radargram of line 30 on the left and interpreted radargram of line 30 on the right showing examples of radar reflector 10, which has been interpreted to represent the undulating angular unconformity contact.

RR11 is interpreted to represent small diameter metal pipes or boulders. The only instance of this type of reflector on a road surface was line 15 across Hardscrabble Road. The remainder of these reflectors were found occurring in the grassy area adjacent to Main Street. Typical examples of this radar reflector can be seen in radargrams 45 and 46 (Figure 21).

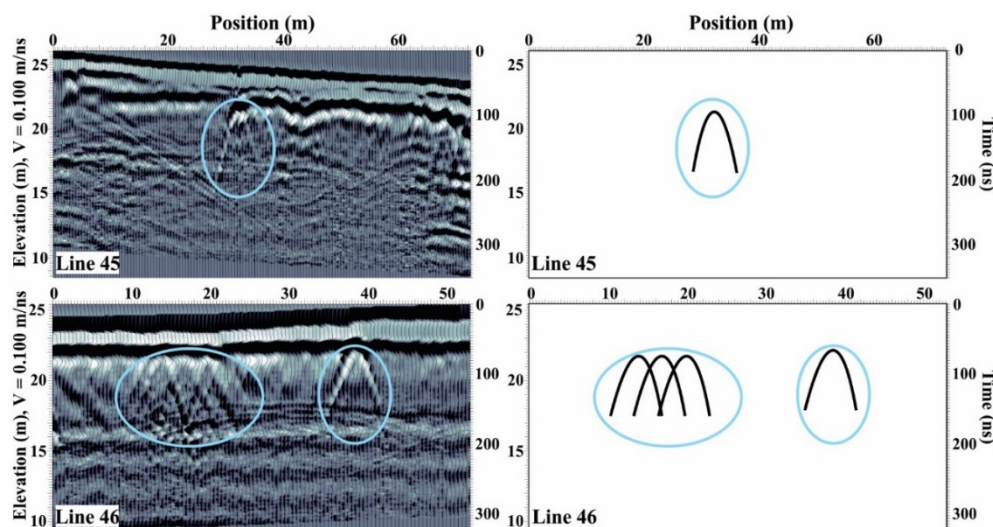


Figure 21. Uninterpreted radargram of line 45 and 46 on the left and interpreted radargram of line 45 and 46 on the right showing examples of radar reflector 11, which is interpreted to represent metal pipes and/or boulders.

RR12 is interpreted to be two instances where data skips occurred (not collected at a trace location). These two vertical features are not related to any subsurface features. The sole example of this radar reflector can be seen in radargram 25 (Figure 22). Despite these two instances of non-signal,

there are noticeable repeating hyperbolae occurring in the background, which correlates to the wooden utility pole at position 75 m near the end of the line.

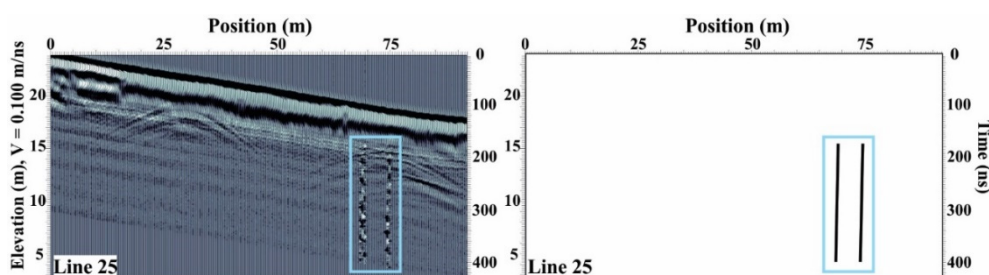


Figure 22. Uninterpreted radargram of line 25 on the left and interpreted radargram of line 25 on the right showing examples of radar reflector 12, which has been interpreted to represent data skips.

RR13 is interpreted to represent the locations of boulders and are associated with the RR2 radar reflector (direct ground wave). Since the area does contain several meters of glacial till, it would be reasonable to assume that larger rocks are present beneath the areas traversed with the GPR. Typical examples of this radar reflector can be seen in radargrams 09 and 10 (Figure 23).

Performing a GPR survey as it was done over the Joggins Formation presented a number of challenges. In the 42 radargrams that were gathered over the study area, it does not appear that any contain reflections that would be considered those of the Joggins Formation. The most probable culprit for the failure in imaging the Joggins Formation strata is the thick clay-rich soil and glacial till overburden that would have greatly attenuated (radar reflector 8) the transmitted energy in the subsurface.

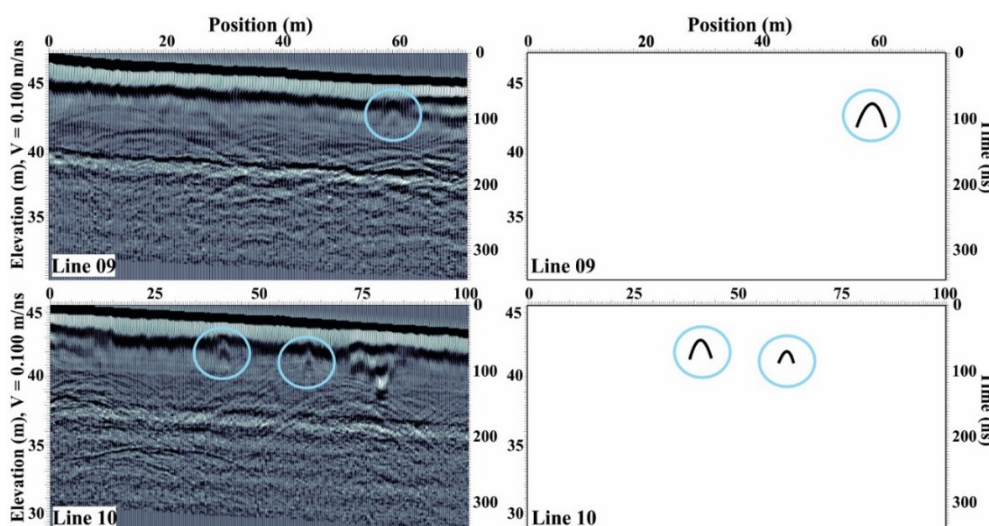


Figure 23. Uninterpreted radargram of line 09 and 10 on the left and interpreted radargram of line 09 and 10 on the right showing examples of radar reflector 13, which is interpreted to represent boulders.

Another probable culprit is the Joggins Formation itself. It is well known from viewing the outcrop on the intertidal area that the strata dip at a constant 21° and are highly variable with respect to both lithology and thickness. Sedimentary beds of a certain thickness would not be visible since they are below the resolution of the antennae used. Furthermore, the beds are composed of a wide range of lithologies, from clay-sized particles up to gravel-sized particles; thus, the individual beds themselves could be contributing to attenuation as well. Power lines run along the edge of the roads that were surveyed, which may result in some problems. At certain sections of the survey, the GPR was near the cliff edge. This could translate into some edge effects in the radargrams.

The GPR data are contaminated to varying degrees by above-ground objects. Several lines were recorded along road surfaces that have regularly spaced wooden utility poles located less than 10 m from the centerline of the road. The data from these lines show regularly spaced and crisp/clear hyperbolae that correlate with the locations of the utility poles along the survey lines. Typical examples are shown in with radar reflector 4. The positions of these hyperbolae correspond with the above-ground positions of two utility poles along the survey line. These similar types of diffraction hyperbolae occur from lines 18 to 25, 27, and 36 collected on Hardscrabble Road, Line 51 collected on Mitchell Street, and lines 42 to 44 collected on Main Street; all of which have power line infrastructure.

In contrast to the regularly spaced utility poles giving regular and clear diffraction hyperbolae, trees on the other hand also cause a similar phenomenon in the radargrams, except that the hyperbolae occur randomly and are overlapping. This theory was tested by viewing the GPR lines that did not have power line infrastructure located next to the road surface, but did have abundant, randomly occurring trees. Typical examples are shown in radar reflector 5, which displays abundant, irregularly spaced and overlapping hyperbolae. Similar diffraction hyperbolae occur in lines 9 to 13 and 31 to 35 on Hardscrabble Road, and Line 43 on Main Street.

In a few instances, a power line will cross over Hardscrabble Road or Main Street. When this occurs, a noticeable feature can be observed in the radargrams (radar reflector 6). The clear and crisp reflectors that are typical with the utility poles become more chaotic. This would infer that the power lines passing overhead do influence the GPR signals.

8. Conclusions

In this study, we have utilized GPR in an attempt to image the internal geometry and architecture of the Joggins Formation and thus, aid with extending the 2D outcrop into 3D by way of modeling the larger scale features. Through iterations of GPR processing techniques and examination of the resulting radargrams, it can be concluded that the survey was unsuccessful in showing Joggins Formation structures and internal architecture. This is likely the result of a combination of factors, with the dominant one being the thick, highly conductive nature of the clay-rich glacial till/overburden. Unfortunately, it was determined that numerous difficulties relating to both the Joggins Formation itself and the area over which the GPR data was collected made any imaging of the Joggins Formation non-occurrence. The imaging issues that are directly related to the Joggins Formation most likely include (1) dipping beds cause increased refraction, unlike a horizontal or nearly horizontal bed, (2) the scale of the beds is too fine for the GPR configuration used for individual beds; at best, it could

only image the thicker beds, and (3) the abundant jointing and fracturing visible in the outcrop exposure probably permeates throughout the subsurface, thereby compounding imaging problems. It is possible that lower frequency antennae could have provided a depth of penetration sufficient to image the Joggins Formation; however, the resolution would have been affected and the likelihood of being able to interpret the dipping strata would have been compromised.

A variety of overburden and surface/subsurface objects may also affect the GPR data collection. Some of the most likely issues include (1) the soil and glacial till making up the overburden layer are clay-rich, thereby leading to signal attenuation, (2) the compacted road surface also has clay materials, in addition to other materials which would also enhance signal attenuation, (3) metallic/wooden objects either exposed at the surface or buried will create additional artifacts in the radargrams. These objects include galvanized steel guard rails, overhead power lines and their associated infrastructure, traffic signage, and cars parked in driveways or passing the GPR equipment while collecting data. Other potential issues that may hamper efforts include the uneven terrain the data was collected on and whether there are GPR data collection issues near the edge of a vertical cliff face. The effects of surface objects, such as trees and utility lines are well-documented as being the culprits of many diffraction hyperbolae seen in the radargrams.

Despite the lack of subsurface imaging from the Joggins Formation, significant insight was gained as to the limitations of the GPR application in this type of environment. There was also some moderate success in imaging the angular unconformity, which was apparent in several radargrams. Perhaps the imaging of the unconformity was related to variations in overburden thickness and/or clay content. Although the primary objective of imaging the Joggins Formation was unsuccessful, it nevertheless increased our knowledge concerning the true impact of clay-rich overburden sediments on bedrock imaging, in addition to the impacts that surface features can cause on GPR data collection. The knowledge gained from this study can be utilized in future GPR surveys, particularly with respect to geoforensic studies where the study areas contain similar surface infrastructure (e.g., utility poles, power lines, etc.). This study also demonstrates the usefulness of shallow subsurface GPR for geohazard assessments. It is important to reiterate that this was the site of extensive past coal mining efforts with well-developed surface infrastructure. Therefore, the area probably contains an abundance of erratic metal objects, large boulders, etc., that would have an influence on the generated radargrams.

Acknowledgments

This work was made possible by the Dalhousie University Basin and Reservoir Laboratory. We are grateful to Bill Richards for overseeing the data collection, data processing and data interpretation aspects, as well as providing helpful suggestions and sound advice for improving this paper. Thanks, must be given to the Basin and Reservoir Laboratory team for their help with field trip arrangements and data collection. We would like to also acknowledge Dr. Lawrence Plug for allowing the use of his GPS equipment. We also thank the anonymous reviewers for their suggestions and comments.

Conflict of interest

All authors declare no conflicts of interest in this paper.

References

1. McMechan GA, Gaynor GC, Szerbiak RB (1997) Use of ground-penetrating radar for 3-D sedimentological characterization of clastic reservoir analogs. *Geophysics* 62: 786–796.
2. Knight R, Tercier P, Jol H (1997) The role of ground penetrating radar and geostatistics in reservoir description. *Leading Edge* 16: 1576–1584.
3. Møller I, Anthony D (2003) A GPR study of sedimentary structures within a transgressive coastal barrier along the Danish North Sea coast. *Geol Soc London Spec Publ* 211: 55–65.
4. Lanzarone P, Garrison E, Bobe R, et al. (2016) Examining Fluvial Stratigraphic Architecture Using Ground-Penetrating Radar at the Fanta Stream Fossil and Archaeological Site, Central Ethiopia. *Geoarchaeology* 31: 577–591.
5. Kostic B, Aigner T (2007) Sedimentary architecture and 3D ground-penetrating radar analysis of gravelly meandering river deposits (Neckar Valley, SW Germany). *Sedimentology* 54: 789–808.
6. Rey J, Martinez J, Hidalgo MC (2013) Investigating fluvial features with electrical resistivity imaging and ground-penetrating radar: The Guadalquivir River terrace (Jaen, Southern Spain). *Sediment Geol* 295: 27–37.
7. Smith DG, Jol HM (1992) Ground-penetrating radar investigation of a Lake Bonneville delta, Provo level, Brigham City, Utah. *Geology* 20: 1–4.
8. Barboza EG, Rosa MLCC, Dillenburg SR, et al. (2014) Stratigraphic analysis applied on the recognition of the interface between marine and fluvial depositional systems. *J Coastal Res* 70: 687–692.
9. Leandro CG, Barboza EG, Caron F, et al. (2019) GPR trace analysis for coastal depositional environments of southern Brazil. *J Appl Geophys* 162: 1–12.
10. Dillenburg SR, Barboza EG, Rosa MLCC, et al. (2017) The complex prograded Cassino barrier in southern Brazil: Geological and morphological evolution and records of climatic, oceanographic and sea-level changes in the last 7–6 ka. *Mar Geol* 390: 106–119.
11. Dillenburg SR, Hesp PA, Keane R, et al. (2020) Geochronology and evolution of a complex barrier, Youngusband Peninsula, South Australia. *Geomorphology* 354: 107044.
12. Neal A (2004) Ground-penetrating radar and its use in sedimentology: principles, problems and progress. *Earth Sci Rev* 66: 261–330.
13. Neal A, Roberts CL (2000) Applications of ground-penetrating radar (GPR) to sedimentological, geomorphological and geoarchaeological studies in coastal environments. In Pye K, Allen JRL, editor. *Coastal and Estuarine Environments: Sedimentology, Geomorphology and Geoarchaeology*, 175: 139–171.
14. Jol HM (2009) *Ground Penetrating Radar Theory and Applications*. In Jol HM, editor. Oxford: Elsevier Science, 545.
15. Jol HM, Smith DG (1991) Ground penetrating radar of northern lacustrine deltas. *Can J Earth Sci* 28: 1939–1947.
16. Beres Jr M, Haeni FP (1991) Application of ground-penetrating-radar Methods in Hydrogeologic Studies. *Groundwater* 29: 375–386.
17. Van Sickle J (2015) *GPS for Land Surveyors*. CRC Press, 368.

18. Gibling MR (2006) Width and thickness of fluvial channel bodies and valley fills in the geological record: A literature compilation and classification. *J Sediment Res* 76: 731–770.
19. Calder JH, Boon J (2007) Joggins Fossil Cliffs: Property Nominated for Inscription on the World Heritage List. Halifax, NS: Nova Scotia Department of Natural Resources, Mineral Resources Branch. Open File Map ME 2007-2001.
20. Calder JH, Gibling MR, Scott AC, et al. (2006) A fossil lycopsid forest succession in the classic Joggins section of Nova Scotia: paleoecology of a disturbance-prone Pennsylvanian wetland. *Geol Soc Am* 399: 169.
21. Davies SJ, Gibling M, Rygel MC, et al. (2005) The Pennsylvanian Joggins Formation of Nova Scotia: sedimentological log and stratigraphic framework of the historic fossil cliffs. *Atl Geol* 41: 115–142.
22. Davies SJ, Gibling MR (2003) Architecture of coastal and alluvial deposits in an extensional basin: the Carboniferous Joggins Formation of eastern Canada. *Sedimentology* 50: 415–439.
23. Rygel MC, Gibling MR, Calder JH (2004) Vegetation-induced sedimentary structures from fossil forests in the Pennsylvanian Joggins Formation, Nova Scotia. *Sedimentology* 51: 531–552.
24. Grey M, Finkel ZV (2011) The Joggins Fossil Cliffs UNESCO World Heritage site: a review of recent research. *Atl Geol* 47: 185–200.
25. Rygel MC, Gibling MR (2006) Natural geomorphic variability recorded in a high-accommodation setting: fluvial architecture of the Pennsylvanian Joggins Formation of Atlantic Canada. *J Sediment Res* 76: 1230–1251.
26. Waldron JWF, Rygel MC (2005) Role of evaporite withdrawal in the preservation of a unique coal-bearing succession: Pennsylvanian Joggins Formation, Nova Scotia. *Geology* 33: 337–340.
27. Carpenter DK, Falcon-Lang HJ, Benton MJ, et al. (2015) Early Pennsylvanian (Langsettian) fish assemblages from the Joggins Formation, Canada, and their implications for palaeoecology and palaeogeography. *Palaeontology* 58: 661–690.
28. Archer AW, Calder JH, Gibling MR, et al. (1995) Invertebrate trace fossils and agglutinated foraminifera as indicators of marine influence within the classic Carboniferous section at Joggins, Nova Scotia, Canada. *Can J Earth Sci* 32: 2027–2039.
29. Reisz R, Modesto SP (1996) Archerpeton anthracos from the Joggins Formation of Nova Scotia: a microsauro, not a reptile. *Can J Earth Sci* 33: 703–709.
30. Tibert NE, Dewey CP (2006) Velatomorpha, a new healdioidean ostracode genus from the early Pennsylvanian Joggins Formation, Nova Scotia, Canada. *Micropaleontology* 52: 51–66.
31. Carroll RL (1967) Labyrinthodonts from the Joggins Formation. *J Paleontol* 41: 111–142.
32. Brand U (1994) Continental hydrology and climatology of the Carboniferous Joggins Formation (lower Cumberland Group) at Joggins, Nova Scotia: evidence from the geochemistry of bivalves. *Palaeogeogr Palaeoclimatol Palaeoecol* 106: 307–321.
33. UNESCO (2008) World Heritage List—Joggins Fossil Cliffs.
34. Falcon-Lang HJ (2009) Earliest history of coal mining and grindstone quarrying at Joggins, Nova Scotia, and its implications for the meaning of the place name “Joggins”. *Atl Geol* 45: 1–20.
35. Rust BR, Gibling MR, Legun AS (1985) Coal deposition in an anastomosing-fluvial system: the Pennsylvanian Cumberland Group south of Joggins, Nova Scotia, Canada. In Rahmani RA, Flores RM, editor. *Sedimentology of Coal and Coal-Bearing Sequences*, 105–120.

36. Quann SL, Young AB, Laroque CP, et al. (2010) Dendrochronological dating of coal mine workings at the Joggins Fossil Cliffs, Nova Scotia, Canada.
37. Google Maps (2020) Google basemap of Joggins Area. Google.
38. Nowland JL, MacDougall JI (1973) Nova Scotia Soil Survey-Soils of Cumberland County Nova Scotia. Canada Department of Agriculture, editor. Ottawa: D.W. Friesen and Sons Ltd., 154.
39. Keys K, Neily P, Quigley E (2010) *Forest Ecosystem Classification for Nova Scotia (Part II: Soil Types)*. Resources NSDoN, editor. Halifax, Nova Scotia: Nova Scotia Department of Natural Resources, 121.
40. Prothero DR, Schwab F (2003) *Sedimentary Geology : An Introduction to Sedimentary Rocks and Stratigraphy*. Freeman & Company, W&H. 600.
41. Stea RR, Finck PW (1986) Surficial Geology, Chigneto Peninsula, Nova Scotia (Sheet 9). Geological Survey of Canada, Map 1630A.
42. Ryan RJ, Calder JH, Donohoe Jr. HV, et al. (1987) Late Paleozoic Sedimentation and Basin Development Adjacent to the Cobequid Highlands Massif, Eastern Canada. In: Beaumont C, Tankard AJ, editors. *Memoir 12—Sedimentary basins and basin-forming mechanisms*. Halifax: Atlantic Geoscience Society, 311–317.
43. RPS Energy (2010) Screening of Potential CO₂ Storage Sites Onshore Nova Scotia. Carbon Capture and Storage Research Consortium of Nova Scotia.
44. Ryan RJ, Boehner RC (1994) *Geology of the Cumberland Basin, Cumberland, Colchester and Pictou Counties, Nova Scotia*. Mines and Energy Branch. Halifax: Department of Natural Resources.
45. Browne GH, Plint AG (1994) Alternating braidplain and lacustrine deposition in a strike-slip setting: The Pennsylvanian Boss Point Formation of the Cumberland Basin, Maritime Canada. *J Sediment Res* 64: 40–59.
46. Martel TA (1987) Seismic Stratigraphy and Hydrocarbon Potential of the Strike-Slip Sackville Sub-Basin, New Brunswick. In: Beaumont C, Tankard AJ, editors. *Memoir 12—Sedimentary basins and basin-forming mechanisms*. Halifax: Atlantic Geoscience Society, 319–334.
47. Allen JP, Fielding CR, Rygel MC, et al. (2013) Deconvolving Signals of Tectonic and Climatic Controls From Continental Basins: An Example From the Late Paleozoic Cumberland Basin, Atlantic Canada. *J Sediment Res* 83: 847–872.
48. Kelly TB, Wach GD (2020) Analysis of factors influencing the interpretation of a digitally examined fluvial meanderbelt system: Joggins Formation, Nova Scotia. *Can J Earth Sci* 57: 524–541.
49. Rygel MC (2005) Alluvial sedimentology and basin analysis of carboniferous strata near Joggins, Nova Scotia, Atlantic Canada. Halifax, NS: Dalhousie University.
50. Gibling MR, Calder JH, Ryan R, et al. (1992) Late Carboniferous and early Permian drainage patterns in Atlantic Canada. *Can J Earth Sci* 29: 338–352.
51. Szymczyk M, Szymczyk P (2013) Preprocessing of GPR data. *Image Process Commun* 18: 83–90.
52. Dojack L (2012) Ground Penetrating Radar Theory, Data Collection, Processing, and Interpretation: A Guide for Archaeologist. University of British Columbia: University of British Columbia, Laboratory of Archaeology, 94.

53. Annan AP (2003) *Ground Penetrating Radar Principles, Procedures & Applications*. Sensors and Software Inc.
54. Annan AP (1999) Practical Processing of GPR Data. Sensors and Software Inc., 1–18.
55. Google (2013) Streetview. Google Inc.
56. Ékes C, Friele P (2003) Sedimentary architecture and post-glacial evolution of Cheekye fan, southwestern British Columbia, Canada. *Geol Soc London Spec Publ* 211: 87–98.
57. Heteren SV, Fitzgerald DM, Mckinlay PA, et al. (1998) Radar facies of paraglacial barrier systems: coastal New England, USA. *Sedimentology* 45: 181–200.



AIMS Press

© 2021 the Author(s), licensee AIMS Press. This is an open access article distributed under the terms of the Creative Commons Attribution License (<http://creativecommons.org/licenses/by/4.0>)